

# A viscoelastic model for turbulent flow over undulating topography

By QINGPING ZOU†

Institute of Geophysics and Planetary Physics, University of California, San Diego, La Jolla, CA 92093-0225, USA

(Received 10 May 1996 and in revised form 10 June 1997)

A viscoelastic model (a mixing-length model with relaxation) is developed to investigate the effect of turbulent advection on the mean flow perturbation and the drag force induced by turbulent shear flow over an undulating surface. The relaxation term is proportional to the ratio of eddy turnover time to travelling time; accordingly, near the surface, the relaxation model reduces to an eddy-viscosity or mixing-length model, while far from the surface it reduces to a rapid-distortion model.

The linear governing equations are transformed into streamline coordinates and solved through matched asymptotic expansions. According to order-of-magnitude estimates in Belcher, Newley & Hunt (1993), the drag force contributed by nonlinear shear stress is of the same order as that contributed by asymmetric pressure arising from the leeward thickening of the perturbed boundary layer. The nonlinear analysis in the present model confirms this estimate in most cases. Our analytical results show a dip in shear stress at the interface between the inner and outer layers and provide evidence that this dynamical feature is related to eddy advection. Numerical calculation using a shooting method gives results that compare well with the analysis.

---

## 1. Introduction

The mean flow, shear stress, pressure perturbations and drag induced by turbulent flow of a homogeneous inviscid fluid over two-dimensional undulating topography have been analysed by Jackson & Hunt (1975), Sykes (1980), Britter, Hunt & Richards (1981), Hunt, Leibovich & Richards (1988, hereinafter referred to as HLR), Belcher, Newley & Hunt (1993, hereinafter referred to as BNH) (see BNH for background reference). Various Reynolds-averaging closure models have been constructed to describe the turbulent motion in this problem: mixing-length models, eddy-viscosity models and higher-order closure models. Speziale (1991) gave a thorough review on these models.

It has been noticed that analogies exist between Newtonian turbulent flow and non-Newtonian laminar flow (see Rivlin 1957 and Speziale 1991). Both Saffman (1977) and Speziale (1987) proposed a nonlinear  $\kappa$ - $\epsilon$  model that includes the eddy viscoelastic properties. Their models are empirically parameterized and are not well suited for analytical development. In this present work, we take a fresh look at this problem by using a different model that is simpler but sophisticated enough to incorporate eddy viscoelasticity.

BNH, like their predecessors, posit a mixing-length model in the inner region (near

† Present address: Department of Oceanography, Dalhousie University, Halifax, Nova Scotia, B3H 4J1, Canada.

the surface) but argue that a rapid-distortion model is more appropriate in the outer region, and neglect the Reynolds stresses in the outer regions when they extended HLR's analysis to obtain a drag force formula. The resulting discontinuity in the Reynolds stresses implies difficulties, which we avoid through a viscoelastic model (see Bradshaw, Ferris & Atwell 1967; Davis 1972; Townsend 1972 and 1976, §7.13):

$$T_e \frac{D\tau}{Dt} + \tau = \tau_e \equiv \nu(u_z + w_x), \quad (1.1)$$

where  $T_e$  is an eddy relaxation time,  $\tau$  is the shear stress,  $\tau_e$  is the corresponding shear stress in the first-order closure models with a Boussinesq viscosity  $\nu$ , and  $u$  and  $w$  are mean velocities. In the turbulent boundary layer, the eddy evolution time scale is  $1/U_z$ , which suggests

$$T_e = \frac{1}{a_1 U_z}, \quad (1.2)$$

where  $a_1$  is a constant and  $U_z$  is the mean velocity shear. We assume an eddy viscosity conserved along streamlines (cf. Miles 1993; van Duin & Janssen 1992):

$$\nu = l^{1+n} u_*^{1-n} \left| \frac{\partial u}{\partial z} \right|^n, \quad (1.3)$$

where  $n$  is an integer distinguishing different models,  $h_B$  is the surface elevation and  $l = \kappa(z - h_B)$  is a mixing length. Equation (1.3) reduces to the eddy viscosity model  $\nu = \kappa(z - h_B) u_*$  when  $n = 0$  and to Prandtl's mixing-length model  $\nu = \kappa^2(z - h_B)^2 |\partial u / \partial z|$  when  $n = 1$ . A viscoelastic model similar to (1.1)–(1.3) is derived by neglecting the diffusion term in Townsend's turbulent energy equation (cf. Appendix A).

Both HLR's and BNH's analyses include nonlinear inertial effects in the middle layer, but inconsistently ignore them in the other layers. In the present model, by applying an integral-equation formulation to the outer domain, we obtain matched solutions of inner and outer layers without introducing the middle layer, which is required by HLR's and BNH's analyses. Moreover, by going to second order in an expansion in powers of the bottom slope, we derive leading-order nonlinear approximations that are uniformly valid in the whole domain. Through order-of-magnitude estimation, BNH predicted that nonlinear shear stress contributes to the drag force at the same order as asymmetric pressure; nonetheless, they ignored it in their drag force derivation. The present nonlinear approximation confirms this estimate in most cases.

Our objective is to apply the viscoelastic closure to the Reynolds-averaged Navier–Stokes equations, examine the turbulent flow over undulating topography with small slopes, and calculate the effect of eddy advection in this problem. We present our work in the following order. In §2, we discuss the general dynamics and associated equations of this problem. Using matched asymptotic expansions, we then derive linear solutions to these equations in §3, and discuss nonlinearity and calculate its leading-order approximation in §4. An analytical formula for the drag force is obtained in §5. We apply a shooting method to the linear perturbation equations in §6. Finally, comparisons of computational results with analytical, experimental, observational, and numerical ones using a second-order closure model are presented in §7 with a discussion. And in §8, we conclude this paper by reviewing the main findings of this study and discuss extending the present model to turbulent flow over a travelling water waves (cf. Zou 1995, Chap. 1, §8).

## 2. General dynamics and governing equations

We consider here the turbulent flow over a hill assuming that  $L/D \ll 1$ ,  $h_0/L \ll 1$  and  $\varepsilon = u_* / \kappa V \ll 1$ , where  $h_0$  and  $L$  are the height and characteristic length of the hill,  $D$  is the turbulent boundary layer (Ekman layer) depth,  $u_*$  is the friction velocity,  $\kappa$  is von Kármán's constant, and  $V$  is the wind speed at an altitude of  $O(L)$  (see figure 1). We neglect separation and buoyancy effects in this problem. Only the lower one-tenth of the boundary layer (wall layer) is of interest for this study, and the Earth's rotation is negligible. We further assume that the approaching turbulent flow is neutrally stable and fully developed; hence the shear stress is constant through the wall layer, and the unperturbed mean flow obeys the logarithmic law:

$$U(z) = \frac{u_*}{\kappa} \log \left( 1 + \frac{z}{z_0} \right) = \begin{cases} \frac{u_*}{\kappa} \log \frac{z}{z_0}, & z \gg z_0, \\ \frac{u_*}{\kappa} \frac{z}{z_0}, & z \rightarrow z_0, \end{cases} \quad (2.1 a)$$

$$(2.1 b)$$

where  $z_0$  is a roughness length (cf. Townsend 1976, §5.9). For an aerodynamically smooth surface,  $z_0$  is proportional to the viscous layer thickness, i.e.  $z_0 = (\nu_k / u_*) \exp(-5\kappa)$ , where  $\nu_k$  is kinematic viscosity; for an aerodynamically rough surface,  $z_0$  is about one-tenth of the average height of the roughness elements. We note that the mean flow (2.1 *a, b*) satisfies the no-slip condition at the surface.

At first order, the mean flow (2.1 *a, b*) is displaced by the streamlines. As a result, the perturbed mean flow becomes

$$U(z-h) = \frac{u_*}{\kappa} \log \frac{z-h}{z_0}, \quad (2.1 c)$$

where  $h = h(x, z)$  is the vertical streamline displacement from its position  $(x, z)$  in the unperturbed flow, which equals  $h_B(x)$  at the surface ( $z \rightarrow z_0$ ) and is zero far from the surface ( $z \rightarrow \infty$ ). Accordingly, we introduce the following streamline coordinates (cf. Miles 1993):

$$\xi = x, \quad \eta = z - h(\xi, \eta). \quad (2.2 a, b)$$

As illustrated in figure 2, the  $\eta$  in (2.2 *b*) is equal to the height at which a streamline originates upstream and is related to its stream function by

$$\Psi(\eta) = \int_0^\eta U(\xi) d\xi, \quad (2.3)$$

where  $U$  is the mean velocity defined in (2.1 *c*) which may be rewritten as

$$U(\eta) = \frac{u_*}{\kappa} \log \left( 1 + \frac{\eta}{z_0} \right) \quad (2.4)$$

in the streamline coordinates. According to (2.3), the coordinate transformation (2.2 *a, b*) is equivalent to von Mises transformation  $(x, z) \rightarrow (x, \Psi)$  (cf. Zeman & Jensen 1987). In these coordinates, each streamline coincides with a constant coordinate  $\eta$ -line, and the controlling equations are homogeneous, so that their solutions are easier to pursue.

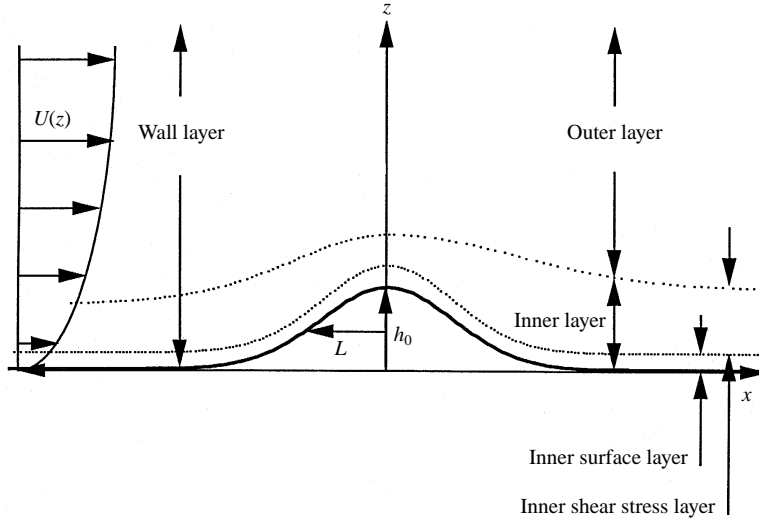


FIGURE 1. Schematic of turbulent flow over a hill showing the three layers with different dynamics (vertical scale is exaggerated).

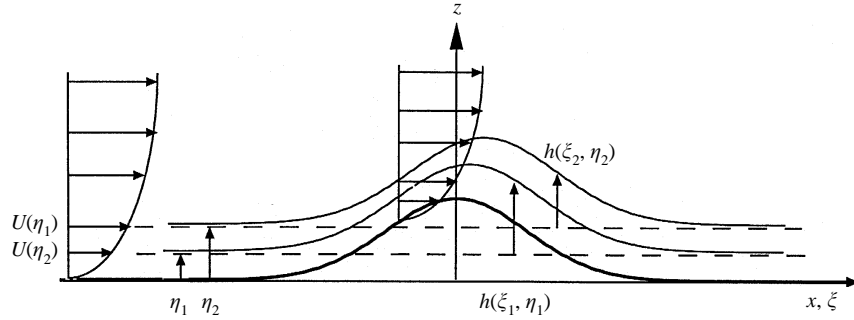


FIGURE 2. Illustration of streamline coordinates and the zeroth-order mean velocity profile  $U(\eta)$  (vertical scale is exaggerated).

In their analyses, BNH also defined a displaced coordinate for each wavenumber  $k$ :

$$\xi = x + \frac{1}{ik} h_B(k) e^{-k\eta}, \quad \eta = z - h_B(k) e^{-k\eta}, \quad (2.5a, b)$$

where the vertical coordinate displacement  $h$  in (2.2b) is replaced by the streamline displacement of the potential flow  $h_B(k) e^{-k\eta}$ , and  $h_B(k)$  is the Fourier transform of topography function  $h_B(x)$ . The dependence of these coordinates on  $k$  renders them more complicated and unsuitable for studying nonlinear effects.

Following Jackson & Hunt (1975), HLR, Jacobs (1987), Jenkins (1992) and Miles (1993), we neglect the molecular viscous effects in this problem so that the following analysis is valid for  $z > z_v$ , where  $z_v = \nu_k / \kappa u_* = O(\varepsilon^{-1} Re^{-1} L)$  is the viscous layer thickness at which kinematic viscosity  $\nu_k$  becomes comparable to eddy viscosity  $\kappa u_* z$ , and  $Re = VL / \nu_k$  is the Reynolds number of the boundary layer. At very high Reynolds numbers, the viscous layer is very thin compared with boundary layer thickness, i.e.  $z_v \ll L$ , and it has minor influence on the dynamics of the full turbulent region.

To find the solutions to this problem, in the following subsections we transform the Reynolds-averaged Navier–Stokes equations into the streamline coordinates, non-dimensionalize and linearize them, and Fourier-transform the linear equations. The resultant equations, combined with a viscoelastic closure model, lead to a governing equation with the Fourier transform of  $h(\xi, \eta)$ ,  $H(k, \eta)$ , as the only unknown variable. Using matched asymptotic expansions, we then obtain the analytical solution  $H(k, \eta)$  in §3.

2.1. *The general dynamics*

The  $x$ - and  $z$ -components of the Reynolds-averaged Navier–Stokes equations are

$$\frac{Du}{Dt} = -\left\langle \frac{p}{\rho} \right\rangle_x - \langle u'^2 \rangle_x - \langle u'w' \rangle_z, \quad (2.6a)$$

$$\frac{Dw}{Dt} = -\left\langle \frac{p}{\rho} \right\rangle_z - \langle w'^2 \rangle_z - \langle u'w' \rangle_x, \quad (2.6b)$$

where  $u \equiv \langle u \rangle$  and  $w \equiv \langle w \rangle$  are the mean velocity components,  $p$  is the mean pressure,  $\rho$  is the density,  $u'$  and  $w'$  are randomly fluctuating velocities in the  $x$ - and  $z$ -directions,  $\langle \rangle$  implies a  $y$ -average, and the subscripts  $x$  and  $z$  signify partial differentiation. Invoking the corresponding transformation of the gradient operator and the substantial derivative,

$$\nabla \equiv [\partial_x, \partial_z] = [\partial_\xi - (1+h_\eta)^{-1}h_\xi\partial_\eta, (1+h_\eta)^{-1}\partial_\eta], \quad (2.7a)$$

and

$$\frac{D}{Dt} \equiv \partial_t + \mathbf{q} \cdot \nabla = \partial_t + u\partial_\xi, \quad (2.7b)$$

assuming steady flow so that  $\partial_t \equiv 0$ , we rewrite (2.6a, b) in the streamline coordinates as

$$uu_\xi = -\left(\pi_\xi - \frac{\pi_\eta h_\xi}{1+h_\eta}\right) + \left(\sigma_\xi - \frac{\sigma_\eta h_\xi}{1+h_\eta}\right) + \frac{\tau_\eta}{1+h_\eta}, \quad (2.8a)$$

$$uw_\xi = -\frac{\pi_\eta}{1+h_\eta} - \frac{\sigma_\eta}{1+h_\eta} + \tau_\xi - \frac{\tau_\eta h_\xi}{1+h_\eta}, \quad (2.8b)$$

where subscripts  $\xi$  and  $\eta$  represent  $\partial_\xi$  and  $\partial_\eta$ ,

$$\pi = \frac{p}{\rho} + \frac{1}{3}\langle u'_i u'_i \rangle, \quad \tau = -\langle u'w' \rangle, \quad \sigma = \left\langle \frac{1}{3}u'_i u'_i - u'^2 \right\rangle = -\left\langle \frac{1}{3}u'_i u'_i - w'^2 \right\rangle. \quad (2.9a-c)$$

Here, repeated indices indicate summation over 1 and 3,  $\pi$ ,  $\rho\sigma$  and  $\rho\tau$  are the modified pressure, deviatoric normal stress and shear stress, and  $\frac{1}{3}\langle u'_i u'_i \rangle$  is the mean square of the velocity fluctuation. Both (2.8a) and (2.8b) include extra terms that are associated with the coordinate transformation and are negligible far from the surface where the streamline displacement  $h(\xi, \eta)$  is very small.

Applying the gradient operator (2.7a) to the stream function (2.3) yields the associated velocity components as

$$u = \frac{U(\eta)}{1+h_\eta}, \quad w = \frac{U(\eta)h_\xi}{1+h_\eta}. \quad (2.10a, b)$$

It is worth emphasizing that the velocity fields in the form of (2.10*a, b*) satisfy the continuity equation automatically, which simplifies the subsequent development.

The boundary conditions follow from no-slip and no-normal-flow conditions at the surface and the requirement of finite energy at the top of the boundary layer, i.e.

$$u, w = 0 \quad \text{as } z \rightarrow z_0, \quad u - U, w, \pi, \tau, \sigma = 0 \quad \text{as } z \rightarrow \infty. \quad (2.11a-g)$$

In the following section §2.2, we will introduce a viscoelastic closure model that relates  $\tau$  and  $\sigma$  to  $u$  and  $w$ , which complements (2.8)–(2.11).

## 2.2. The viscoelastic model

We hypothesize a viscoelastic eddy model (cf. Bradshaw *et al.* 1967; Davis 1972; Townsend 1972 and 1976, §7.13):

$$T_e \frac{D\tau}{Dt} + \tau = \tau_e \equiv \nu(\bar{u}_z + w_x) \quad (2.12a)$$

and

$$T_e \frac{D\sigma}{Dt} + \sigma = \sigma_e \equiv 2\nu u_x \equiv -2\nu w_z, \quad (2.12b)$$

where  $T_e = 1/(a_1 U_\eta)$ ,  $a_1 = -\langle u'w' \rangle / q^2 = 0.15$  is the ratio between shear stress  $-\langle u'w' \rangle$  and turbulent energy  $q^2$ ,  $\tau_e$  and  $\sigma_e$  are the corresponding shear stress and normal stress in the first-order closure models with a Boussinesq viscosity  $\nu$ . We note that  $T_e = \kappa\eta / (a_1 u_*) = l / (a_1 u_*)$ , which is proportional to the ratio of mixing length and friction velocity, i.e. the characteristic length scale and velocity of turbulent motion, is an eddy relaxation time. Neglecting the diffusion term in Townsend's turbulent energy equation, we derive a viscoelastic model similar to (2.12) (see Appendix A).

Van Duin & Janssen (1992) consider first-order closure models for which

$$\nu = l^{1+n} u_*^{1-n} \left| \frac{\partial u}{\partial z} \right|^n, \quad (2.13a)$$

where  $n$  is an integer distinguishing different models,  $l = \kappa(z - h_B)$  is a mixing length,  $h_B$  is the surface elevation; (2.13*a*) reduces to the eddy viscosity model  $\nu = \kappa(z - h_B) u_*$  when  $n = 0$  and Prandtl's mixing-length model  $\nu = \kappa^2(z - h_B)^2 |\partial u / \partial z|$  when  $n = 1$ . Instead, to incorporate the effect of streamline distortion, we hypothesize the mixing length

$$l = \kappa(z - h) = \kappa\eta \quad (2.13b)$$

which is conserved along streamlines  $\eta = \text{constant}$  (see Townsend 1972 and Miles 1993).

Applying the gradient operator and substantial derivative (2.7*a, b*) to (2.12*a, b*) leads to

$$T_e u \tau_\xi + \tau = \nu \left( \frac{u_\eta}{1 + h_\eta} + w_\xi - \frac{w_\eta h_\xi}{1 + h_\eta} \right) \quad (2.14a)$$

and

$$T_e u \sigma_\xi + \sigma = -2\nu \frac{w_\eta}{1 + h_\eta}, \quad (2.14b)$$

in which nonlinear inertial terms are retained to be consistent with their inclusion in the momentum equations (2.8*a, b*).

## 2.3. Non-dimensional governing equations and boundary conditions

For simplicity, we non-dimensionalize (2.8a, b) and (2.14a, b) by the scalings

$$h_B \rightarrow h_0 h_B, \quad h \rightarrow h_0 h, \quad (\xi, \eta) \rightarrow L(\xi, \eta), \quad (u, w) \rightarrow V(u, w), \quad (2.15 a-d)$$

$$U \rightarrow VU, \quad \tau \rightarrow V^2 \mu \tau, \quad \pi \rightarrow V^2 \mu \pi, \quad \nu \rightarrow \frac{\nu}{VL}, \quad (2.15 e-h)$$

where  $h_0$  is the height of the hill,  $V$  is the mean velocity at  $\eta = L$ ,  $\mu = h_0/L$  and  $\varepsilon = u_*/(\kappa V)$  are the basic small parameters of the problem (typical values of  $\varepsilon$  are 0.03–0.07 in the atmospheric boundary layer), and invoke the non-dimensional velocity fields in (2.10a, b):

$$u = \frac{U}{1 + \mu h_\eta}, \quad w = \frac{\mu U h_\xi}{1 + \mu h_\eta}, \quad (2.16 a, b)$$

assuming  $\mu = h_0/L$  is small and omitting nonlinear terms of  $O(\mu^2)$ , we then have

$$-U^2 h_{\xi\eta} = \tau_\eta - \pi_\xi + \sigma_\xi, \quad \pi_\eta = -U^2 h_{\xi\xi} - \sigma_\eta + \tau_\xi, \quad (2.17 a, b)$$

$$\alpha \frac{U}{U_\eta} \tau_\xi + \tau = \tau_e, \quad \alpha \frac{U}{U_\eta} \sigma_\xi + \sigma = \sigma_e, \quad (2.17 c, d)$$

where

$$\tau_e = \tau_0 - \frac{\nu}{U} (U^2 h_\eta)_\eta + \nu_0 U h_{\xi\xi}, \quad \sigma_e = -2\nu_0 (U h_\xi)_\eta, \quad (2.18 a, b)$$

the zeroth-order non-dimensional eddy viscosity  $\nu$  is given by

$$\nu_0 = \varepsilon \kappa^2 \eta, \quad \nu = (n+1) \nu_0, \quad \alpha = \frac{1}{a_1} = \frac{1}{0.15}, \quad (2.19 a-c)$$

$$U = \varepsilon \log \frac{\eta}{z_0} \quad (2.19 d)$$

is the dimensionless mean velocity, and

$$\tau_0 = \nu_0 U_\eta = (\varepsilon \kappa)^2 \quad (2.19 e)$$

is the dimensionless zeroth-order constant shear stress for  $n = 0$ . It follows from  $V = U^*(L)$ , where superscript  $*$  denotes a dimensional variable, that  $U(1) = 1$  and  $\varepsilon = -\log \eta_0$ , where  $\eta_0 = z_0/L$  is a dimensionless roughness length.

Combined with (2.16a, b), (2.11a–d) gives the boundary conditions for  $h$  and  $h_\eta$ , i.e.

$$h = h_B, \quad U h_\eta = 0 \quad \text{as } \eta \rightarrow \eta_0, \quad h = 0, \quad h_\eta = 0 \quad \text{as } \eta \rightarrow \infty. \quad (2.20 a-d)$$

Substituting (2.18a, b) into (2.17c, d), and introducing Fourier transforms with respect to  $\xi$ ,

$$\begin{aligned} & [H(k, \eta), H_B(k), \Pi(k, \eta), T(k, \eta), \Sigma(k, \eta)] \\ &= \int_{-\infty}^{\infty} [h(\xi, \eta), h_B(\xi), \pi(\xi, \eta), \tau(\xi, \eta) - \tau_0, \sigma(\xi, \eta)] \exp(-ik\xi) d\xi, \end{aligned} \quad (2.21)$$

we obtain

$$-ikU^2 H_\eta = T_\eta + ik(\Sigma - \Pi), \quad \Pi_\eta = k^2 W^2 H - \Sigma_\eta + ikT, \quad (2.22 a, b)$$

$$T = \frac{-(\nu/U)(U^2 H_\eta)_\eta - k^2 \nu_0 UH}{1 + ik\alpha U/U_\eta}, \quad \Sigma = \frac{-2ik\nu_0(UH)_\eta}{1 + ik\alpha U/U_\eta}, \quad (2.22 c, d)$$

and the boundary conditions (2.20a–d) transform to

$$H = H_B, \quad UH_\eta = 0 \quad \text{as } \eta \rightarrow \eta_0, \quad H = 0, \quad H_\eta = 0 \quad \text{as } \eta \rightarrow \infty, \quad (2.23a-d)$$

where  $k$  is the dimensionless wavenumber. The presence of argument lists  $(k, \eta)$  and  $(k)$  denotes the Fourier transform of the corresponding variable and will be dropped hereinafter for convenience.

For sinusoidal topography of wavenumber  $k$ , we may proceed in the same manner, but with a different inverse Fourier transform

$$\begin{aligned} [h(\xi, \eta), h_B(\xi), \pi(\xi, \eta), \tau(\xi, \eta) - \tau_0, \sigma(\xi, \eta)] \\ = \text{Re} \{ [H(k, \eta), H_B(k), \Pi(k, \eta), T(k, \eta), \Sigma(k, \eta)] \exp(ik\xi) \}. \end{aligned} \quad (2.24)$$

### 3. Analytical solutions

Following Jackson & Hunt (1975), Sykes (1980) and HLR, we use the matched asymptotic expansions to seek the solutions to this problem. We divide the whole domain above the surface into three layers: outer layer, inner shear stress layer and inner surface layer, in each of which different dynamics governs, and the perturbation shear stress is  $O(\varepsilon^2)$ ,  $O(\varepsilon^1)$ ,  $O(\varepsilon^0)$  respectively. Solutions to equations (2.22a–d) will be constructed for each layer and eventually matched.

#### 3.1. Inner shear stress layer

A balance between the inertial and shear stress terms in (2.22a) provides the estimate of the thickness of the inner layer  $l$ , namely

$$l \log \frac{l}{\eta_0} = (n+1) \kappa^2, \quad (3.1)$$

where  $\eta_0$  is the roughness length, and  $n$  is the integer introduced in the first-closure models (cf. (2.13a)). We emphasize that all the following length variables such as  $l$  and  $\eta_0$  have been non-dimensionalized with respect to  $L$ . In the atmosphere, the thickness of the inner layer is typically much smaller than that of the turbulent boundary layer but much larger than the roughness length, i.e.  $\eta_0 \ll l \ll 1$  (see figure 3a). It then is appropriate to introduce the stretched coordinate

$$\hat{\eta} = \eta/l \quad (3.2)$$

and the small parameter

$$\delta \equiv \frac{u_*}{\kappa U(l)} = \frac{1}{\log(l/\eta_0)}, \quad (3.3a)$$

which is related to the small parameter  $\varepsilon$  by

$$\delta = \frac{\varepsilon}{U(l)} \quad \text{or} \quad \delta = \frac{\varepsilon}{1 + \varepsilon \log l} \quad (3.3b, c)$$

and  $l$  by

$$\delta = \frac{l}{(n+1) \kappa^2} \quad (3.3d)$$

according to (3.1) (see figure 3b, c).

The dimensionless mean velocity  $U$  is thus related to the stretched coordinate  $\hat{\eta}$  by

$$U = U(l) (1 + \delta \log \hat{\eta}), \quad (3.4)$$

where  $U(l) = 1 + \varepsilon \log l$  is the value of  $U$  at the top of the inner layer where  $\eta = l$ .



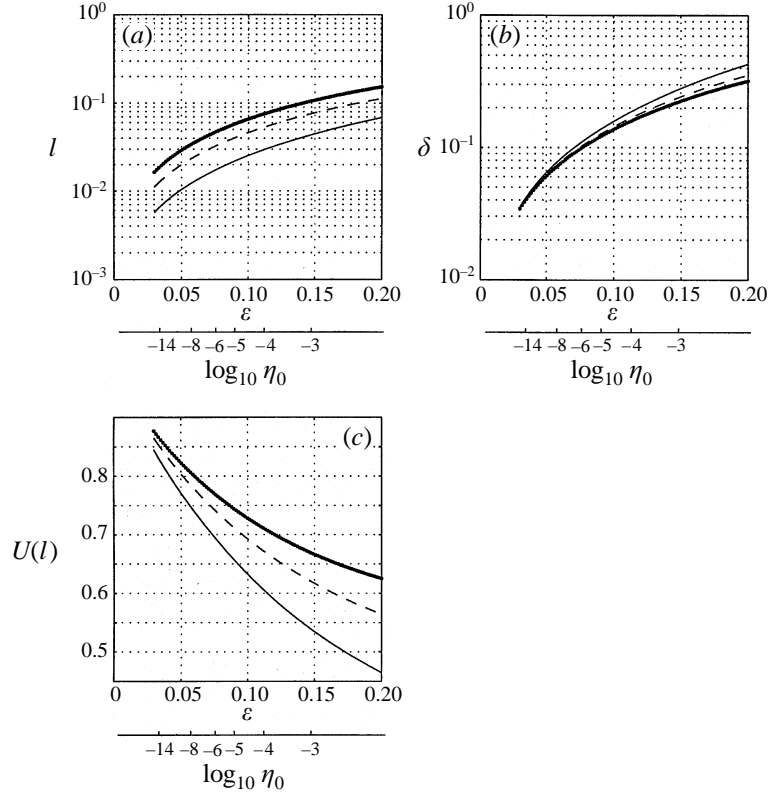


FIGURE 3. Variation of (a) inner shear-stress-layer thickness  $l$ , (b) small parameter  $\delta$  and (c) dimensionless mean velocity at the top of inner layer  $U(l)$  with dimensionless roughness length  $\eta_0$  and small parameter  $\varepsilon$ . —,  $n = 0$ ; ---,  $n = 1$ ; — · —,  $n = 2$ .

According to the vertical pressure gradient (2.22 *b*), the pressure  $\Pi$  may be taken as a constant  $\Pi_0(k)$  with an error factor  $1 + O(\delta^2)$ . The  $\Sigma$ -terms are  $O(\delta^2)$  in both (2.22 *a*) and (2.22 *b*) and therefore may also be omitted at  $O(\delta)$ . Omitting  $k^2\nu_0 UH$  of  $O(\delta^2)$  (2.22 *c*) and then substituting it into (2.22 *a*), we have

$$ikU^2 H_\eta = \left[ \frac{(v/U)(U^2 H_\eta)_\eta}{1 + ik\alpha U/U_\eta} \right]_\eta + ik\Pi_0 + O(\delta^2). \quad (3.5)$$

We decompose the solution to (3.5) into the complementary and particular parts, i.e.

$$H_\eta(k, \eta) = \hat{H}_\eta(k, \eta) + \frac{\Pi_0(k)}{U^2}, \quad (3.6a)$$

where according to (3.5),  $\hat{H}_\eta(k, \eta)$  satisfies the homogeneous equation

$$ikU^2 \hat{H}_\eta = \left[ \frac{(v/U)(U^2 \hat{H}_\eta)_\eta}{1 + ik\alpha U/U_\eta} \right]_\eta. \quad (3.6b)$$

Substituting  $U$  from (3.4) into (3.6 *b*), neglecting terms of  $O(\delta^2)$  and invoking (3.2), we transform (3.6 *b*) into an equation with the independent variable  $\hat{\eta}$ :

$$ik\hat{H}_{\hat{\eta}}(k, \hat{\eta}) = \left[ \frac{\hat{\eta}\hat{H}_{\hat{\eta}\hat{\eta}}}{1 + i(n+1)k\alpha\kappa^2\hat{\eta}} \right]_{\hat{\eta}}. \quad (3.7)$$

Integrating (3.7) over  $(\hat{\eta}_0, \hat{\eta})$  yields

$$Y_{\hat{\eta}\hat{\eta}} = \left[ -(n+1)(k\alpha^{1/2}\kappa^2 + \frac{ik}{\hat{\eta}}) \right] Y, \quad (3.8a)$$

where

$$Y(k, \hat{\eta}) = \hat{H}(k, \hat{\eta}) - \hat{H}(k, \hat{\eta} \rightarrow \hat{\eta}_0), \quad (3.8b)$$

and  $\hat{\eta}_0 = \eta_0/l$  is the stretched coordinate of the roughness length  $\eta_0$ . By introducing a new independent variable:

$$\bar{\eta} = 2ik\beta\hat{\eta}, \quad (3.9a)$$

where

$$\beta = ((n+1)\alpha)^{1/2}\kappa, \quad (3.9b)$$

we reduce (3.8a) to Whittaker's equation (see Olver 1974 and Abramowitz & Stegun 1970, §13.1.31),

$$Y_{\bar{\eta}\bar{\eta}} + \left[ -\frac{1}{4} - \frac{1}{2\beta\bar{\eta}} \right] Y = 0. \quad (3.9c)$$

The solution to (3.9c) that vanishes at  $\bar{\eta} \rightarrow \infty$  is

$$Y = C_h \exp(-\frac{1}{2}\bar{\eta}) \bar{\eta} F\left(1 + \frac{1}{2\beta}, 2, \bar{\eta}\right), \quad (3.9d)$$

where  $F$  is a confluent hypergeometric function, and the constant coefficient  $C_h$  is determined by matching with the inner surface layer at the bottom of the inner shear stress layer, where  $\bar{\eta} \rightarrow 0$ .

Differentiating (3.9d) about  $\hat{\eta}$ , and invoking (3.6a) and (3.8b), we obtain

$$H_\eta = \frac{\Pi_0(k)}{U^2} + C_h \exp(-\frac{1}{2}\bar{\eta}) \left[ \frac{1}{2}\bar{\eta} F\left(1 + \frac{1}{2\beta}, 2, \bar{\eta}\right) - F\left(\frac{1}{2\beta}, 1, \bar{\eta}\right) \right], \quad (3.10a)$$

the integration of which over  $(\hat{\eta}_0, \hat{\eta})$  yields

$$H = \frac{\Pi_0}{U^2} \eta \left(1 + \frac{2}{\varepsilon U} + \dots\right) + C_h \eta \exp(-\frac{1}{2}\bar{\eta}) F\left(1 + \frac{1}{2\beta}, 2, \bar{\eta}\right) + C, \quad (3.10b)$$

where the constant coefficient  $C$  is determined by matching with the inner surface layer at the bottom of the inner layer. Near the surface ( $\hat{\eta} \rightarrow \hat{\eta}_0$ ),  $H_\eta$  and  $H$  approach their asymptotic values of

$$H_\eta(k, \hat{\eta} \rightarrow \hat{\eta}_0) = \frac{\Pi_0}{U^2} + C_h \frac{1}{\Gamma(1/2\beta)} \left[ \beta + \phi\left(\frac{1}{2\beta}\right) + 2\gamma + \ln(2ik\beta) + \log \hat{\eta} \right] \quad (3.11a)$$

$$\begin{aligned} &= \frac{\Pi_0}{U^2(l)} (1 - 2\delta \log \hat{\eta}) + C_h \frac{1}{\Gamma(1/2\beta)} \\ &\quad \times \left[ \beta + \phi\left(\frac{1}{2\beta}\right) + 2\gamma + \ln(2ik\beta) + \log \hat{\eta} \right] + O(\delta^2) \end{aligned} \quad (3.11b)$$

and

$$H(k, \hat{\eta} \rightarrow \hat{\eta}_0) = \frac{\Pi_0}{U^2} \eta \left(1 + \frac{2}{\varepsilon U} + \dots\right) + C_h \frac{1}{\Gamma(1/2\beta)} \left[ \eta(\log \hat{\eta} - 1) + \frac{l}{ik} \right] + C \quad (3.11c)$$

$$\begin{aligned} &= \frac{\Pi_0}{U^2(l)} [1 - 2\delta(\log \hat{\eta} - 1)] + C_h \frac{1}{\Gamma(1/2\beta)} \left[ \eta(\log \hat{\eta} - 1) + \frac{l}{ik} \right] + C + O(\delta^2), \\ & \quad (3.11d) \end{aligned}$$

where  $\gamma \doteq 0.577$  is Euler's constant, and  $\Gamma(1/2\beta)$  and  $\phi$  are the gamma and digamma functions respectively. Solutions (3.11 *b, d*) match those of the inner surface layer (see §3.2) only if

$$C_h = \frac{2\delta\Pi_0\Gamma(1/2\beta)}{U(l)^2}, \quad C = H_B - \frac{2\delta l\Pi_0}{ikU^2(l)}, \quad (3.12 a, b)$$

hence (3.11 *a, b*) and (3.11 *c, d*) become

$$H_\eta(k, \hat{\eta}) = \frac{\Pi_0}{U^2} + \frac{2\delta\Pi_0}{U(l)^2} \Gamma\left(\frac{1}{2\beta}\right) \exp\left(-\frac{1}{2}\bar{\eta}\right) \left[ \frac{1}{2}\bar{\eta} F\left(1 + \frac{1}{2\beta}, 2, \bar{\eta}\right) - F\left(\frac{1}{2\beta}, 1, \bar{\eta}\right) \right] \quad (3.13 a)$$

$$= \frac{\Pi_0}{U(l)^2} \left\{ 1 - 2\delta \left[ \log \hat{\eta} - \Gamma\left(\frac{1}{2\beta}\right) \exp\left(-\frac{1}{2}\bar{\eta}\right) \left[ \frac{1}{2}\bar{\eta} F\left(1 + \frac{1}{2\beta}, 2, \bar{\eta}\right) - F\left(\frac{1}{2\beta}, 1, \bar{\eta}\right) \right] \right] \right\} + O(\delta^2) \quad (3.13 b)$$

and

$$H = H_B + \frac{\Pi_0}{U^2} \eta \left( 1 + \frac{2}{\varepsilon U} + \dots \right) + \frac{2\delta\Gamma(1/2\beta)}{U^2(l)} \Pi_0 \eta \exp\left(-\frac{1}{2}\bar{\eta}\right) F\left(1 + \frac{1}{2\beta}, 2, \bar{\eta}\right) - \frac{2\delta l\Pi_0}{ikU^2(l)} \quad (3.13 c)$$

$$= H_B + \frac{\Pi_0}{U^2(l)} \eta \left\{ 1 - 2\delta \left[ \log \hat{\eta} - 1 - \Gamma\left(\frac{1}{2\beta}\right) \exp\left(-\frac{1}{2}\bar{\eta}\right) F\left(1 + \frac{1}{2\beta}, 2, \bar{\eta}\right) \right] \right\} + O(\delta^2). \quad (3.13 d)$$

Differentiating (3.13 *a, b*) with respect to  $\hat{\eta}$  gives

$$H_{\eta\eta}(k, \hat{\eta}) = \frac{-2\Pi_0 U_\eta}{U^3} + \frac{2\delta\Pi_0}{U(l)^2} \Gamma\left(\frac{1}{2\beta}\right) \frac{d\bar{\eta}}{d\hat{\eta}} \exp\left(-\frac{1}{2}\bar{\eta}\right) \left( \frac{1}{4}\bar{\eta} + \frac{1}{2\beta} \right) F\left(1 + \frac{1}{2\beta}, 2, \bar{\eta}\right) \quad (3.13 e)$$

$$= \frac{2\delta\Pi_0}{U(l)^2} \left\{ \frac{1}{\eta} + \Gamma\left(\frac{1}{2\beta}\right) \frac{d\bar{\eta}}{d\hat{\eta}} \exp\left(-\frac{1}{2}\bar{\eta}\right) \left( \frac{1}{4}\bar{\eta} + \frac{1}{2\beta} \right) F\left(1 + \frac{1}{2\beta}, 2, \bar{\eta}\right) \right\} + O(\delta^2), \quad (3.13 f)$$

where  $d\bar{\eta}/d\hat{\eta} = 2ik\beta$ . Near the surface where  $U \rightarrow 0$  ( $\hat{\eta} \rightarrow \hat{\eta}_0$ ), on the right-hand-side of (3.13 *e*), the first term has a singularity, which is cancelled by that of the second term.

We recognize the imaginary term on the right-hand side of (3.13 *c*),  $-2\delta l\Pi_0/ikU^2(l)$ , as an asymmetric component of the vertical streamline displacement  $H$ , which was called leeward streamline thickening by BNH. In the following sections, we show that this term composes the main part of the asymmetric pressure and drag force.

The particular part of the solution  $H_\eta$  in (3.13 *a*), i.e.  $\Pi_0/U^2$ , is the leading-order perturbation to the mean flow within this layer, and is the same as its solution in linear potential flow. A similar conclusion was also drawn by Sykes (1980). In the subsequent section, we show that the leading-order nonlinear corrections to the preceding linear formula are precisely those of nonlinear potential flow, and related to the pressure term  $\Pi$ . It follows then that pressure determines the leading-order perturbation of velocity fields. The same conclusion holds for the outer layer flow (see §3.3). Nevertheless, the Reynolds shear stress accounts for the leading-order  $\eta$ -dependent perturbation, suggesting its key role in energy and momentum exchange between different layers as well as vertical structure of turbulent flow. Moreover, as demonstrated in the next subsection, shear stress determines the leading-order perturbation of velocity fields in the inner surface layer.

### 3.2. Inner surface layer

Within a very thin layer next to the surface where  $\hat{\eta} \rightarrow \hat{\eta}_0$ ,  $\ln \hat{\eta} \rightarrow \ln 1/\hat{\eta}_0 \equiv -\delta^{-1}$ , so that the asymptotic expansions in §3.1 are no longer valid; at the same time  $U \rightarrow 0$  so that a logarithmic singularity appears in solutions (3.13 *a, c, e*). Consequently, we shall approach the problem separately in this region. Following HLR, we call this region the inner surface layer, and assume that the thickness of this layer is about the same order as the roughness length.

Introducing a new variable

$$\Phi(k, \eta) = U^2 H_\eta(k, \eta) - \Pi_0 \quad (3.14a)$$

in (3.5) yields

$$ik\Phi = \left[ \frac{(\nu/U) \Phi_\eta}{1 + ik\alpha U/U_\eta} \right], \quad (3.14b)$$

which may be rewritten as

$$\frac{d}{d\hat{U}} \left( \frac{1}{\hat{U}(1 + ik\alpha\eta_0 \hat{U} \exp(\hat{U}))} \frac{d\Phi}{d\hat{U}} \right) = \frac{ik\eta_0 \exp(\hat{U})}{(n+1)\kappa^2} \Phi, \quad (3.15a)$$

with a new independent variable

$$\hat{U} = U/\varepsilon = \log \eta/\eta_0. \quad (3.15b)$$

Combination of (3.14 *a*) and (2.23 *b*) gives the boundary condition for  $\Phi$  at the surface, i.e.

$$\Phi = \Phi_0 = -\Pi_0 \quad \text{as} \quad \eta \rightarrow \eta_0. \quad (3.16)$$

Through iterative integration, we then obtain the solution of (3.15 *a*), subject to boundary conditions (3.16). We start with approximating (3.15 *a*) by

$$\frac{d}{d\hat{U}} \left( \frac{1}{\hat{U}(1 + ik\alpha\eta_0 \hat{U} \exp(\hat{U}))} \frac{d\Phi}{d\hat{U}} \right) = 0, \quad (3.17)$$

whose solution is found by integration as

$$\text{where} \quad \Phi = \Phi_0 - \frac{T_0}{2(n+1)\kappa^2} [\hat{U}^2 + ik\alpha\eta_0 \exp(\hat{U}) (\hat{U}^2 - 2\hat{U} + 2)], \quad (3.18a)$$

$$T_0 = \frac{-(n+1)\kappa^2}{\hat{U}(1 + ik\alpha\eta_0 \hat{U} \exp(\hat{U}))} \frac{d\Phi}{d\hat{U}} \Big|_{\eta \rightarrow \eta_0} \quad (3.18b)$$

is the shear stress at the surface. It follows that solution (3.18 *a*) corresponds to constant shear stress in the inner surface layer.

Substituting (3.18 *a*) into the right-hand side of (3.15 *a*), integrating it over  $(\eta_0, \eta)$  and omitting terms of  $O(\eta_0)^2$ , we finally obtain

$$\begin{aligned} \Phi = & \Phi_0 - \frac{T_0}{2(n+1)\kappa^2} \{ \hat{U}^2 + ik\alpha\eta_0 [\exp(\hat{U}) (\hat{U}^2 - \hat{U} + 1) - 1] \} \\ & + \frac{ik\eta_0}{(n+1)\kappa^2} \{ \Phi_0 (\hat{U} - 1) \exp(\hat{U}) + \Phi_0 - \left[ \Phi_0 - \frac{T_0}{(n+1)\kappa^2} \right] \frac{\hat{U}^2}{2} \\ & - \frac{T_0}{2(n+1)\kappa^2} (\hat{U}^3 - 5\hat{U}^2 + 12\hat{U} - 12) + \frac{6T_0}{(n+1)\kappa^2} \}. \end{aligned} \quad (3.19)$$

Combination of (3.19) and (3.14a) gives the asymptotic value of  $H_\eta$  as  $\eta \rightarrow l\hat{\eta}$ :

$$H_\eta = -\frac{T_0}{2(n+1)(\varepsilon\kappa)^2} + O(\eta_0) = H_{0\eta} + O(\eta_0), \quad (3.20)$$

where  $H_{0\eta} = -T_0/[2(n+1)(\varepsilon\kappa)^2]$  is a constant proportional to the surface shear stress. Equation (3.20) shows that, at leading order, the perturbation flow fields are determined by the Reynolds shear stress instead of pressure as in the outer and inner shear stress layers, which suggests that different dynamics governs this region and that it is necessary to treat this region separately in this problem.

Matching solution  $H_\eta$  in (3.20) with its inner limit of the shear stress layer, i.e.  $H_\eta(k, \hat{\eta} \rightarrow \hat{\eta}_0)$  in (3.11b), we have

$$T_0 = -2(n+1)(\varepsilon\kappa)^2 U^{-2}(l) \Pi_0 [1 + 2\delta(\beta + \phi(1/2\beta) + 2\gamma + \ln(2ik\beta))] \quad (3.21a)$$

and

$$C_h = \frac{2\delta I(1/2\beta)}{U^2(l)} \Pi_0. \quad (3.21b)$$

We now integrate (3.20) over  $(\eta_0, \eta)$  and obtain

$$H = H_B - H_{0\eta} \eta. \quad (3.22)$$

Matching solution  $H$  in (3.22) with its inner limit of the shear stress layer, i.e.  $H(k, \hat{\eta} \rightarrow \hat{\eta}_0)$  in (3.11d), we also have

$$C = H_B - \frac{2\delta l \Pi_0 \{1 + U_0^2/U^2(l)\}}{ikU^2(l)}, \quad (3.23)$$

where the constant pressure  $\Pi_0$  is further determined by matching the inner and outer solutions of  $H_\eta$  and  $H$  at the interface of the inner and outer layers.

### 3.3. Outer layer

In the outer layer where  $\eta = O(1)$ , the Reynolds stresses are  $O(\varepsilon^2)$  relative to the inertial term and therefore may be neglected to derive solutions with an error factor  $1 + O(\varepsilon^2)$ . The momentum equations (2.22a, b) then reduce to

$$U^2 H_\eta(k, \eta) = \Pi, \quad \Pi_\eta(k, \eta) = k^2 U^2 H, \quad (3.24a, b)$$

where the mean velocity now takes the form

$$U = 1 + \varepsilon \ln \eta. \quad (3.25)$$

According to (3.24a) and (3.24b), the outer flow conserves perturbation vorticity along streamlines, so that the perturbation flow is irrotational on the assumption of zero vorticity in the upstream limit. Previous models (cf. Sykes 1980; HLR) drew similar conclusions on the character of the flow in the outer layer.

Eliminating  $\Pi$  from (3.24a) and (3.24b) leads to

$$(U^2 H_\eta)_\eta - k^2 U^2 H = 0. \quad (3.26)$$

Proceeding as in Appendix C of Miles (1993), we first posit the solution to (3.26) in the form

$$UH = \psi(\eta) \exp(-k\eta), \quad (3.27)$$

and transform (3.26), subject to the outer conditions  $\psi \rightarrow \psi_\infty$ , to the integral equation

$$\psi = \psi_\infty + \frac{1}{2|k|} \int_\eta^\infty \{1 - \exp[-2|k|(\zeta - \eta)]\} U^{-1} U_{\zeta\zeta} \psi \, d\zeta, \quad (3.28)$$

where  $\zeta$  is a dummy variable.

We then obtain the solution of (3.28) through iteration, starting from the first approximation

$$\psi = \psi_\infty + O(\varepsilon). \quad (3.29a)$$

Combining (3.25) and (3.29a) in (3.28), we further derive the second approximation

$$\begin{aligned} \psi &= \psi_\infty \left\{ 1 + \frac{1}{2|k|} \int_\eta^\infty \{1 - \exp[-2|k|(\zeta - \eta)]\} U^{-1} U_{\zeta\zeta} \, d\zeta \right\} \\ &= \psi_\infty \left\{ 1 - \int_\eta^\infty \exp[-2|k|(\zeta - \eta)] U_\zeta \, d\zeta + O(\varepsilon^2) \right\} \\ &= \psi_\infty [1 - \varepsilon \exp(2|k|\eta) E_1(2|k|\eta) + O(\varepsilon^2)], \end{aligned} \quad (3.29b)$$

where  $E_1$  is the exponential integral (cf. Abramowitz & Stegun 1970, §5). Hence altogether from (3.25), (3.27) and (3.29b), we have now the following solutions:

$$H(k, \eta) = H_\infty \{1 - \varepsilon [E_1(2|k|\eta) \exp(2|k|\eta) + \ln \eta] + O(\varepsilon^2)\} \exp(-|k|\eta), \quad (3.30a)$$

$$H_\eta(k, \eta) = -H_\infty |k| \{1 + \varepsilon [E_1(2|k|\eta) \exp(2|k|\eta) - \ln \eta] + O(\varepsilon^2)\} \exp(-|k|\eta), \quad (3.30b)$$

where  $H_\infty$  is a constant coefficient to be determined by matching outer and inner solutions. We note that from their maximum value at the top of inner shear stress layer, the solutions (3.30a, b) decay exponentially to zero as  $\eta \rightarrow +\infty$  and therefore satisfy boundary conditions (2.23c, d) there.

#### 3.4. Matching inner and outer solutions

We next derive the coefficients  $\Pi_0$  through matching the inner limits of the outer-layer solutions  $H$  and  $H_\eta$  in (3.30a, b) with the outer limits of the inner-layer solutions  $H$  and  $H_\eta$  in (3.11a, c).

From the outer-layer solutions (3.30a, b), we have the asymptotic behaviours of  $H$  and  $H_\eta$  at  $\eta \rightarrow l\hat{\eta}$ , namely

$$H(k, \eta \rightarrow l\hat{\eta}) = H_\infty [1 - |k| l\hat{\eta} + \varepsilon(\gamma + \ln 2|k|) + \varepsilon |k| l\hat{\eta}(\gamma + \ln 2|k| + 2 \ln l + 2 \ln \hat{\eta} - 2)] \quad (3.31a)$$

and

$$H_\eta(k, \eta \rightarrow l\hat{\eta}) = -H_\infty |k| [1 - \varepsilon(\gamma + \ln 2|k| + 2 \ln l + 2 \ln \hat{\eta})], \quad (3.31b)$$

where  $\gamma = 0.577 \dots$  is Euler's constant. Similarly, from the inner-layer solutions (3.13a, c), we also have the asymptotic behaviours of  $H$  and  $H_\eta$  at  $\hat{\eta} \rightarrow \infty$ , namely

$$H(k, \hat{\eta} \rightarrow \infty) = H_B + \Pi_0 \eta [1 - 2\varepsilon(\ln \eta - 1)] - \frac{2\delta l \Pi_0}{ik U^2(l)} \quad (3.32a)$$

$$= H_B + \frac{\Pi_0}{U^2(l)} \eta [1 - 2\delta(\ln \hat{\eta} - 1)] - \frac{2\delta l \Pi_0}{ik U^2(l)} + O(\delta^2) \quad (3.32b)$$

and

$$H_\eta(k, \hat{\eta} \rightarrow \infty) = \Pi_0 (1 - 2\varepsilon \ln \eta) = \frac{\Pi_0}{U^2(l)} (1 - 2\delta \ln \hat{\eta}) + O(\delta^2). \quad (3.32c, d)$$

Matching (3.31 *b*) with (3.32 *c*) then gives

$$\Pi_0 = -|k| H_\infty [1 - \varepsilon(\gamma + \ln 2 |k|)]. \quad (3.33)$$

Matching (3.31 *a*) with (3.32 *a, b*) and invoking (3.33 *a*) leads to

$$H_\infty = H_B \left[ 1 - \varepsilon(\gamma + \ln 2 |k|) + \varepsilon^2(\gamma + \ln 2 |k|)^2 + \frac{2|k|\delta l}{ikW(l)^2} (1 - 3\varepsilon(\gamma + \ln 2 |k|)) \right] \quad (3.34a)$$

$$= H_B \left[ 1 - \varepsilon(\gamma + \ln 2 |k|) + \varepsilon^2(\gamma + \ln 2 |k|)^2 + \frac{2|k|\delta l}{ik} (1 - \varepsilon(\gamma + \ln 2 |k|) - 2\varepsilon \ln l) \right]. \quad (3.34b)$$

Substituting (3.34 *a, b*) into (3.33) thus gives the constant pressure term

$$\Pi_0(k) = -H_B |k| \left[ 1 - 2\varepsilon(\gamma + \ln 2 |k|) + 2\varepsilon^2(\gamma + \ln 2 |k|)^2 + \frac{2|k|\delta l}{ikW(l)^2} (1 - 4\varepsilon(\gamma + \ln 2 |k|)) \right] \quad (3.35a)$$

$$= -H_B |k| \left[ 1 - 2\varepsilon(\gamma + \ln 2 |k|) + 2\varepsilon^2(\gamma + \ln 2 |k|)^2 + \frac{2|k|\delta l}{ik} (1 - 2\varepsilon(\gamma + \ln 2 |k| + \ln l)) \right], \quad (3.35b)$$

whose imaginary part is

$$\text{Im}(\Pi_0(k)) = 2(n+1)(\varepsilon\kappa)^2 W(l)^{-4} H_B k [1 - 4\varepsilon(\gamma + \ln 2 |k|)] \quad (3.35c)$$

$$= 2(n+1)(\varepsilon\kappa)^2 W(l)^{-2} H_B k [1 - 2\varepsilon(\gamma + \ln 2 |k| + \ln l)]. \quad (3.35d)$$

### 3.5. Structure of turbulence

From the shear-stress formula (2.17 *c*) or (2.17 *d*), we may estimate the height where turbulent advection becomes important compared to turbulent production and dissipation by

$$\alpha \frac{U}{U_\eta} = 1 \quad (3.36)$$

which, together with (2.19 *c*) and (2.19 *d*), gives

$$\eta_a \log \frac{\eta_a}{\eta_0} = a_1 = 0.15, \quad (3.37)$$

where  $\eta_a$  is the height at which the first-order closure models become invalid. The relaxation time for eddies is  $T_e = 1/a_1 U_\eta$ , the time required for eddies to pass over the topography is  $T_t = 1/U$ , so that the ratio of these two time scales is  $T_e/T_t = U/(a_1 U_\eta) = \alpha U/U_\eta$ . Near the surface where  $\eta < \eta_a$  we have  $T_e/T_t = \alpha U/U_\eta > 1$ , namely eddies evolve in a time scale  $T_e$  smaller than their travelling time  $T_t$ ; hence they attain local equilibrium, and the viscoelastic model (2.12) reduces to a first-order closure model  $\tau = \tau_e = \nu(u_z + w_x)$ . On the other hand, far away from the surface where  $\eta > \eta_a$  we have  $T_e/T_t = \alpha U/U_\eta < 1$ , namely that within their travelling time  $T_t$  eddies are only weakly perturbed by the undulation of topography, so that  $D\tau/Dt \rightarrow 0$ , i.e. shear stress is conserved along streamlines, and the viscoelastic model reduces to rapid-distortion theory.

Invoking  $\alpha \approx 1/\kappa^2$ , we find that (3.1) reduces to (3.37) for  $n = 0$ , so that  $l \approx \eta_a$ , namely eddy advection becomes important at the top of the inner layer. This result is conceivable from the fact that the vertical structure of the turbulent flow couples with that of the mean flow.

#### 4. Nonlinear correction

From the solutions  $H$ ,  $H_\eta$  and  $H_{\eta\eta}$  in (3.13 *a, c, e*), we estimate that the linear components of pressure, inertia and Reynolds stress terms in the governing equations (2.8 *a, b*) are  $O(1)$ ,  $O(1)$  and  $O(\delta)$ ; the nonlinear components of these terms are  $O(\mu)$  relative to their linear components and, therefore, are  $O(\mu)$ ,  $O(\mu)$  and  $O(\delta\mu)$  respectively. It follows that the leading-order nonlinear equation in this problem is made up of only nonlinear terms associated with pressure and inertia; that is, it takes the same form as that of potential flow. Omitting the Reynolds stress terms in (2.8 *a*) and (2.8 *b*) leads to

$$-U^2 h_{\xi\eta} = -\pi_\xi (1 + \mu h_\eta)^3 + \mu \pi_\eta h_\xi (1 + \mu h_\eta)^2, \quad \pi_\eta = U^2 \left( \frac{h_\xi}{1 + \mu h_\eta} \right)_\xi. \quad (4.1 a, b)$$

We now substitute (4.1 *b*) into (4.1 *a*) and obtain the Bernoulli equation

$$\left[ \frac{1}{2} \left( \frac{U}{1 + \mu h_\eta} \right)^2 + \frac{1}{2} \left( \frac{\mu U h_\xi}{1 + \mu h_\eta} \right)^2 + \mu \pi \right]_\xi = 0. \quad (4.2)$$

Assuming that the perturbation to the mean flow vanishes in the upstream limit and integrating (4.2) over  $(-\infty, \xi)$ , we obtain

$$\left( \frac{U}{1 + \mu h_\eta} \right)^2 + \left( \frac{\mu U h_\xi}{1 + \mu h_\eta} \right)^2 + 2\mu \pi = U^2. \quad (4.3)$$

Assuming a small topographic slope  $\mu$ , we expand the perturbation variables  $h_\xi$ ,  $h_\eta$  and  $\pi$  in powers of  $\mu$ , i.e.

$$h_\eta = h_\eta^{(0)} + \mu h_\eta^{(1)} + O(\mu^2), \quad h_\xi = h_\xi^{(0)} + \mu h_\xi^{(1)} + O(\mu^2), \quad \pi = \pi^{(0)} + \mu \pi^{(1)} + O(\mu^2). \quad (4.4 a-c)$$

Substituting (4.4 *a-c*) into (4.3), at  $O(\mu^0)$  we then have

$$h_\eta^{(0)} = \frac{\pi^{(0)}}{U^2}, \quad (4.5 a)$$

and at  $O(\mu^1)$  we then have

$$h_\eta^{(1)} = \frac{1}{2}\mu \left[ (h_\xi^{(0)})^2 + 3 \frac{(\pi^{(0)})^2}{U^4} \right]. \quad (4.5 b)$$

As we argued at the beginning of this section, formulas (4.5 *a*) and (4.5 *b*) are valid with an error factor  $1 + O(\delta)$ , even if we consider Reynolds stresses. Combined with (4.5 *a*), (4.5 *b*) yields

$$h_\eta^{(1)} = \frac{1}{2}[3(h_\eta^{(0)})^2 + (h_\xi^{(0)})^2], \quad (4.6)$$

which is used to derive the leading-order nonlinear correction to the drag force in the next section.

#### 5. Drag force

Both the pressure and the Reynolds stresses at the surface contribute to the perturbation force exerted on the topography, which is given by the following integration along the surface:

$$D_i = -\rho \int_{-\infty}^{\infty} (\sigma_{ij} - p\delta_{ij})_{\eta=\eta_0} n_j dl, \quad (5.1 a)$$



where  $\rho$  is the density,  $p$  is the pressure,  $\sigma_{ij}$  is the Reynolds stress tensor, and  $n_j$  is the unit normal vector of the surface. The topographical drag force is given by the horizontal component of (5.1 *a*), namely

$$D = \rho \int_{-\infty}^{\infty} [\tau - \tau_0 + h_{\xi}(\pi - \sigma)]_{\eta=\eta_0} d\xi [1 + O(\mu^2)], \quad (5.1 b)$$

where  $\rho\tau_0 = \rho u_*^2$  is the zeroth-order shear stress. Equation (5.1 *b*) indicates that the drag force comes from the perturbation shear stress, the pressure and normal stress in phase with the slope of the topography. Using the scalings (2.15 *a-g*), we non-dimensionalize (5.1 *b*) as

$$\frac{D}{\rho V^2 L} = \mu \int_{-\infty}^{\infty} [\tau - \tau_0 + \mu h_{\xi}(\pi - \sigma)]_{\eta=\eta_0} d\xi + O(\mu^2), \quad (5.1 c)$$

which may be decomposed into three components:

$$\left\{ \frac{D_{\tau}}{\rho V^2 L}, \frac{D_{\sigma}}{\rho V^2 L}, \frac{D_{\pi}}{\rho V^2 L} \right\} = \mu \int_{-\infty}^{\infty} \{(\tau - \tau_0), -\mu h_{\xi} \sigma, \mu h_{\xi} \pi\}_{\eta=\eta_0} d\xi + O(\mu^2). \quad (5.2 a-c)$$

BNH, Sykes and others showed that the drag force from the linear shear stress is zero, which will be confirmed next. Hence, the leading-order drag force is  $O(\mu^2)$  and comprises contributions from the nonlinear shear stress, the linear normal stresses and linear pressure. The previous analyses by BNH and others are linear, and nonlinear shear stress is implicitly neglected in their drag force calculations without verification; therefore, it is desirable to test this assumption by computations.

Substituting (2.18 *a*) and (2.18 *b*) into (2.17 *c*) and (2.17 *d*), invoking (4.4 *a, b*), and considering that the mean velocity is zero at the surface, we obtain

$$\begin{aligned} \frac{D_{\tau}}{\rho V^2 L} &= -\mu(\varepsilon\kappa)^2 \int_{-\infty}^{\infty} \{(n+1)[2h_{\eta} - (2n+3)\mu h_{\eta}^2] + \mu h_{\xi}^2\}_{\eta=\eta_0} d\xi \\ &= -\mu(\varepsilon\kappa)^2 \int_{-\infty}^{\infty} \{2(n+1)h_{\eta}^{(0)} + \{(n+1)[2h_{\eta}^{(1)} - (2n+3)\mu(h_{\eta}^{(0)})^2] \\ &\quad + \mu(h_{\xi}^{(0)})^2\}_{\eta=\eta_0} d\xi, \end{aligned} \quad (5.3 a)$$

$$\frac{D_{\sigma}}{\rho V^2 L} = 2\mu^2(\varepsilon\kappa)^2 \int_{-\infty}^{\infty} (h_{\xi}^{(0)})^2 \Big|_{\eta=\eta_0} d\xi + O(\mu^3), \quad (5.3 b)$$

$$\frac{D_{\pi}}{\rho V^2 L} = \mu^2 \int_{-\infty}^{\infty} (h_{\xi}^{(0)} \pi^{(0)})_{\eta=\eta_0} d\xi + O(\mu^3), \quad (5.3 c)$$

where superscripts (0) and (1) imply the linear and nonlinear parts of the variable. The sum of (5.3 *a*) and (5.3 *b*) give the contribution of the deviatoric Reynolds stresses

$$\frac{D_{\tau} + D_{\sigma}}{\rho V^2 L} = -\mu(\varepsilon\kappa)^2 \int_{-\infty}^{\infty} \{2(n+1)h_{\eta}^{(0)} + \{(n+1)[2h_{\eta}^{(1)} - (2n+3)\mu(h_{\eta}^{(0)})^2] - \mu(h_{\xi}^{(0)})^2\}_{\eta=\eta_0} d\xi. \quad (5.4)$$

Combined with the Fourier transform of (2.21), the linear part of (5.4) reduces to

$$\frac{D_l}{\rho V^2 L} = \frac{D_{\tau} + D_{\sigma}}{\rho V^2 L} = -2(n+1)(\varepsilon\kappa)^2 (2\tilde{\pi})^{-1} H_{\eta}(k, \eta) \Big|_{\eta=\eta_0}, \quad (5.5)$$

where  $\tilde{\pi} = 3.14159\dots$ . Combining (3.21 *a*) and (3.34 *a*), and invoking (3.20), we obtain

$$H_\eta|_{\eta=\eta_0} = -H_B |k| W(l)^{-2} \{1 - 2\varepsilon(\gamma + \ln 2 |k|) + 2\delta[\beta + \phi(1/2\beta) + 2\gamma + \ln(2ik\beta)]\}, \quad (5.6)$$

which yields  $D_l/(\rho V^2 L) = 0$ , i.e. the linear Reynolds stresses do not contribute to the drag force.

Combined with the leading-order nonlinear correction (4.6), the nonlinear part of (5.4) reduces to

$$\frac{D_n}{\rho V^2 L} = \frac{D_\tau + D_\sigma}{\rho V^2 L} = n(\varepsilon\kappa)^2 \mu^2 \int_{-\infty}^{\infty} [2(n+1)(h_\eta^{(0)})^2 - (h_\xi^{(0)})^2]_{\eta=\eta_0} d\xi, \quad (5.7a)$$

which becomes zero when  $n = 0$  (the eddy viscosity model), and

$$\frac{D_n}{\rho V^2 L} = \frac{D_\tau + D_\sigma}{\rho V^2 L} = (\varepsilon\kappa)^2 \mu^2 \int_{-\infty}^{\infty} [4(h_\eta^{(0)})^2 - (h_\xi^{(0)})^2]_{\eta=\eta_0} d\xi, \quad (5.7b)$$

when  $n = 1$  (the mixing-length model).

Applying Parseval's theorem to (5.3 *c*), and using  $\Pi_0$  in (3.35 *c*) as the Fourier transform of pressure at the surface, we obtain the contribution of pressure to the drag force as

$$\begin{aligned} \frac{D_\pi}{\rho V^2 L} &= \mu^2 (2\tilde{\pi})^{-1} \int_{-\infty}^{\infty} (-ik H^* \Pi_0)_{\eta=\eta_0} dk + O(\mu^3) \\ &= 2(n+1) \mu^2 (\varepsilon\kappa)^2 U(l)^{-4} (2\tilde{\pi})^{-1} \int_{-\infty}^{\infty} k^2 [1 - 4\varepsilon(\gamma + \ln 2 |k|)] |H_B|^2 dk + O(\mu^3), \end{aligned} \quad (5.8)$$

where the superscript \* denotes the complex conjugate, and  $H_B$  is the Fourier transform of the non-dimensional surface elevation  $h_B$ . For sinusoidal topography with wavenumber  $k$  and complex amplitude  $H_B$ , the drag force formula (5.8) reduces to

$$\begin{aligned} \frac{D_\pi}{\rho V^2 L} &= \frac{1}{2} \text{Re}(-ik H_B^* \Pi_0) + O(\mu^3) \\ &= 2(n+1) \mu^2 (\varepsilon\kappa)^2 U(l)^{-4} [1 - 4\varepsilon(\gamma + \ln 2 |k|)] k^2 |H_B|^2 + O(\mu^3). \end{aligned} \quad (5.9)$$

Invoking the scalings (2.15) and

$$V = U(L) = \frac{u_*}{\kappa} \ln \frac{L}{z_0} = \frac{u_*}{\varepsilon\kappa}, \quad (5.10)$$

we now dimensionalize (5.9) and obtain

$$D_\pi = C_\pi \rho u_*^2 \int_{-\infty}^{\infty} h_{B\xi}^2(\xi) d\xi, \quad (5.11a)$$

where  $h_{B\xi}$  is the surface slope,

$$C_\pi = 2(n+1) [1 - 4\varepsilon(\gamma + \ln 2 |k|)] \frac{1}{U^4(l)} = 2(n+1) \frac{U^4(\eta_1)}{U^4(l)}, \quad (5.11b)$$

and

$$\eta_1 = \frac{1}{2k} \exp(-\gamma). \quad (5.11c)$$

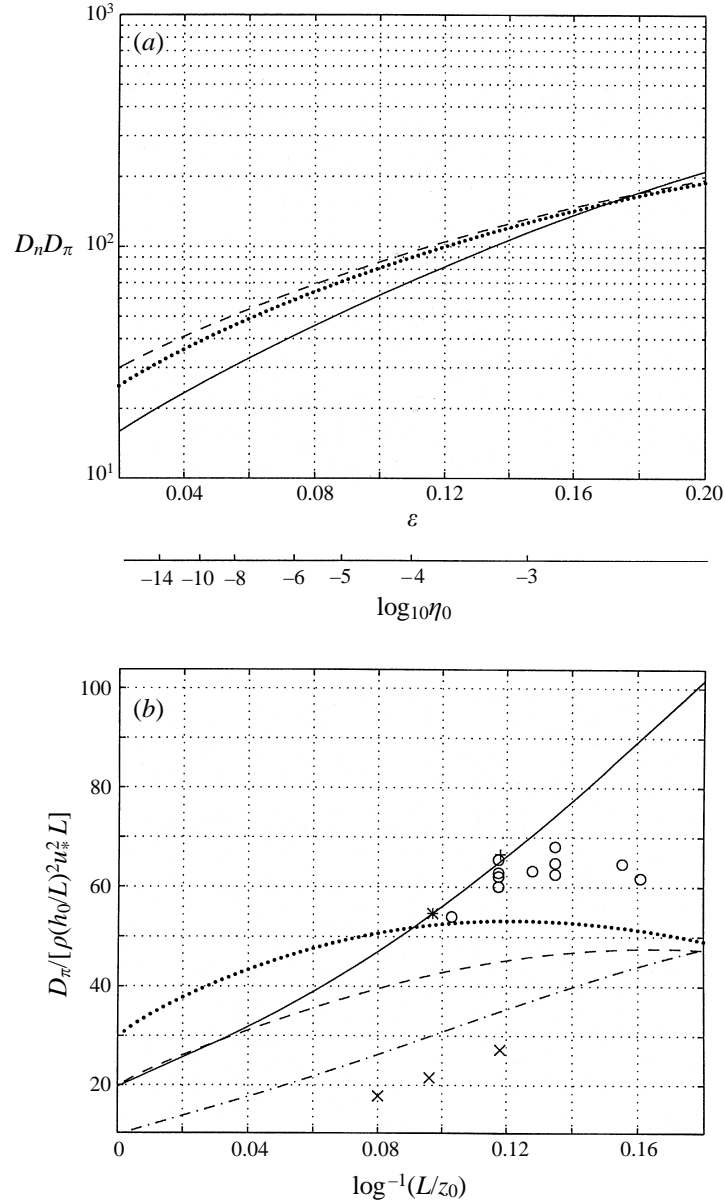


FIGURE 4. (a) The perturbation drag force  $D_\pi$  due to pressure and  $D_n$  due to nonlinear shear stress as a function of dimensionless roughness length  $\eta_0$  and small parameter  $\epsilon$  for a sinusoidal terrain with wavenumber  $k = \frac{1}{2}\pi$  (equations (5.11 a) and (5.14 a), terms of  $O(\epsilon)$  are omitted in calculation). —,  $D_\pi$  for  $n = 0$ ; ---,  $D_\pi$  for  $n = 1$ ;  $\cdots$ ,  $D_n$  for  $n = 1$ . (b) Perturbation drag force on a sinusoidal terrain with wavenumber  $k = \frac{1}{2}\pi$ : analytical results of present model (5.11 a) for  $\cdots$ ,  $n = 2$ ; ----,  $n = 1$ ; -.-,  $n = 0$ ; —, BNH's truncated mixing-length model;  $\circ$ , BNH's numerical computation of second-order closure model; +, Townsend's (1980) numerical model; \*, Zilker & Hanratty's (1979) experiment; x, Townsend's (1972) numerical model.

For comparison, we list the formula for  $C_\pi$  from some previous authors:

$$C_\pi = 2 \left[ \ln \frac{1}{kz_0} - C \right] \begin{cases} C = 0 & \text{(Knight 1977; Jacobs 1987),} \\ C = \gamma + \ln 2 & \text{(Miles 1993),} \end{cases} \quad (5.12a)$$

$$C_\pi = 4 \quad \text{(Sykes 1980),} \quad (5.12b)$$

$$C_\pi = \frac{4}{U^4(l)} \quad \text{(BNH; Belcher & Hunt 1993).} \quad (5.12c)$$

If Sykes (1980), BNH and Belcher & Hunt (1993) had followed Knight (1977), Jacobs (1987) and Miles (1993), and used an eddy-viscosity model instead of a mixing-length model in their studies, the factor 4 in (5.12b) and (5.12c) would vanish. Moreover, since  $\ln(1/kz_0) = O(\varepsilon^{-1})$ , formula (5.12a) predicts a drag that is about  $\frac{1}{2}\varepsilon^{-1}$  larger than (5.12b, c), which is the result of applying first-order closure models to both inner and outer layers.

Applying Parseval's theory to (5.7a) yields

$$\frac{D_n}{\rho V^2 L} = n(\varepsilon k)^2 \mu^2 (2\tilde{\pi})^{-1} \int_{-\infty}^{\infty} [2(n+1)|H_\eta|_{\eta=\eta_0}^2 - |kH_B|^2] dk + O(\mu^3). \quad (5.13)$$

Invoking (5.6) and (5.13) and introducing

$$D_n = C_n \rho u_*^2 \int_{-\infty}^{\infty} h_{B\xi}^2(x) dx, \quad (5.14a)$$

we obtain

$$C_n = n \frac{1}{U^4(l)} [2(n+1)(1+4\delta B) - 1], \quad (5.14b)$$

where

$$B = \beta + \phi(1/2\beta) + \gamma + \ln(\beta). \quad (5.14c)$$

We illustrate the linear and nonlinear drag force for sinusoidal topography in figure 4(a); it shows that the drag force due to nonlinear shear stress and linear normal stress  $D_n$  is of about the same order as that due to asymmetric pressure  $D_\pi$ . This conclusion contradicts most previous studies but is consistent with that of Jacobs (1989) who pointed out that neglect of nonlinearity in this problem may lead to an underestimate of the form drag. Figure 4(b) shows that the calculated  $D_n$  for  $n=2$  and  $n=1$  agree fairly well with BNH's numerical results and Zilker & Hanratty's (1979) observational results, whereas  $D_\pi$  for  $n=0$  is close to Townsend's (1972) numerical results.

## 6. Numerical calculation

Jenkins (1992) showed that  $\varepsilon = 0.03\text{--}0.07$  (typical values in the atmospheric boundary layer) is not small enough for an asymptotic analysis to be accurate. We now calculate the solutions to this problem numerically in order to check the reliability of our analytical results. We will write the linear momentum equations (2.22a) and (2.22b) and constitutive equations (2.22c) and (2.22d) as first-order differential equations with real variables and coefficients, estimate  $\text{Re}(H_\eta)$ ,  $\text{Im}(H_\eta)$ ,  $\text{Re}(II)$  and  $\text{Im}(II)$  at the surface, and then employ a shooting method that combines an initial value program for solving ordinary differential equations and a multi-dimensional root finding program (see Sanford & Shipman 1972).

Equations (2.22a–c) could be transformed into a set of eight coupled first-order

differential equations with dependent real variables:  $\text{Re}(H)$ ,  $\text{Im}(H)$ ,  $\text{Re}(H_\eta)$ ,  $\text{Im}(H_\eta)$ ,  $\text{Re}(T)$ ,  $\text{Im}(T)$ ,  $\text{Re}(II)$ ,  $\text{Im}(II)$  and independent variable  $\eta$ , which is done in Appendix B.

According to (2.23 *a*) and (2.22 *c*), the lower boundary conditions at the surface become

$$\begin{cases} \text{Re}(H) = H_B \\ \text{Im}(H) = 0 \end{cases} \quad \text{and} \quad \begin{cases} \text{Re}(T) = -2(n+1)(\varepsilon\kappa)^2 \text{Re}(H_\eta) \\ \text{Im}(T) = -2(n+1)(\varepsilon\kappa)^2 \text{Im}(H_\eta) \end{cases} \quad \text{at} \quad \eta \rightarrow \eta_0. \quad (6.1 a)$$

The upper boundary conditions (2.23 *c, d*), required by the finite energy condition, become

$$\begin{cases} \text{Re}(H) = 0 \\ \text{Im}(H) = 0 \end{cases} \quad \text{and} \quad \begin{cases} \text{Re}(H_\eta) = 0 \\ \text{Im}(H_\eta) = 0 \end{cases} \quad \text{at} \quad \eta \rightarrow +\infty. \quad (6.2 a)$$

Since the boundary conditions at the surface are not complete, we cannot integrate the equations directly. It is therefore expedient to pursue the solutions through a shooting method. The shooting procedure involves the following steps. Four estimated values are assigned to  $\text{Re}(H_\eta)$ ,  $\text{Im}(H_\eta)$ ,  $\text{Re}(II)$  and  $\text{Im}(II)$  at the lower boundary, i.e.

$$\text{Re}(H_\eta) = -kH_B, \quad \text{Re}(II_0) = -kH_B, \quad (6.3 a)$$

$$\text{Im}(H_\eta) = 0, \quad \text{Im}(II_0) = 2(n+1)(\varepsilon\kappa)^2 kH_B, \quad (6.3 b)$$

and together with (6.1 *a, b*), they make up a complete set of boundary conditions. The corresponding initial value problem (*B 1 a-h*) is solved using the HIPREC integration routine. The estimates (6.3) are then perturbed and used to derive another set of solutions. By observing the discrepancy between these two sets of solutions in satisfying boundary conditions (6.2) at some large  $\eta_L$  and applying multi-dimensional root finding Newton–Raphson method, the trial estimates (6.3) can be refined iteratively. The solutions to linear equations are derived in just one iteration. The integration routine adjusts the grid size automatically to satisfy the requirement of tolerance. We used  $10^{-11}$  as the initial value of tolerance and found that the solutions are not sensitive to a change around this value. In the above procedure, we apply the lower boundary conditions at some small value  $\eta = \eta_s$  to avoid the singularity at  $\eta = \eta_0$ , and the values of  $\eta_s$  and  $\eta_L$  are adjusted until the solutions are not sensitive to their change.

The analytical and numerical results obtained here so far apply only to a sinusoidal topography; however, the same procedure could (in principle) be carried out for the Fourier components of different wavenumbers to determine the solutions for a hill with arbitrary shape and mild slope.

## 7. Results and comparisons

As we mentioned in §1, there have been many studies on turbulent flow over a hill. This problem was approached either analytically by eddy-viscosity and mixing-length models or numerically by higher-order Reynolds-stress-closure schemes. The experimental and numerical results of Zeman & Jensen (1987) both showed a dip in the Reynolds stress at a height where the maximum speed-up occurs. They pointed out that this is a remarkable aspect of the dynamics that is left out by current analytical models. In their computation of the Reynolds stress profile, BNH used a second-order closure model. Consequently, it is of interest to compare our analytical and numerical results,

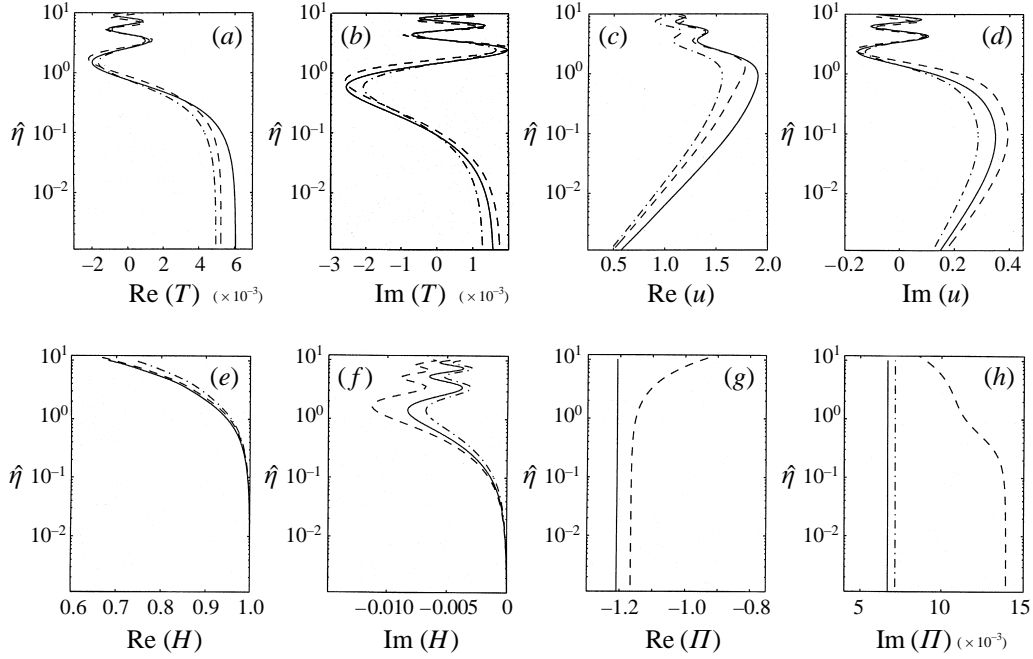


FIGURE 5. Comparisons of analytical and numerical results for a roughness length  $\eta_0 = 2 \times 10^{-6}$ , wavenumber  $k = \frac{1}{2}\pi$  and  $n = 0$  ( $l \approx 0.018$ ,  $\delta \approx 0.11$ ,  $\varepsilon \approx 0.076$ ): —, analytical solutions with matching coefficient (3.35a); - · -, analytical solutions with matching coefficient (3.35b); - · - · -, numerical calculation. (a)  $\text{Re}(T)$ , (b)  $\text{Im}(T)$ , (c)  $\text{Re}(u)$ , (d)  $\text{Im}(u)$ , (e)  $\text{Re}(H)$ , (f)  $\text{Im}(H)$ , (g)  $\text{Re}(II)$ , (h)  $\text{Im}(II)$ .

and with those others, and then use these results to quantitatively resolve the effect of eddy advection on the dynamics of turbulent motion.

In order to justify our analytical approximations, we first compare our analytical and numerical results for sinusoidal topography  $h_B = \text{Re}(\exp(ik\xi))$ . Combining (3.13) and (3.35), invoking (2.16a) and (2.22c) and with the dimensionless wavenumber  $k = \frac{1}{2}\pi$ , we calculate the analytical solutions of  $H$ ,  $H_\eta$  and  $H_{\eta\eta}$ ,  $II$ ,  $u$  and  $T$  in the inner shear stress layer. Figure 5 compares the analytical and numerical-integration calculations for a roughness length  $\eta_0 = 2 \times 10^{-6}$  and  $n = 0$  ( $l \approx 0.018$ ,  $\delta \approx 0.11$ ,  $\varepsilon \approx 0.076$ ). The real and imaginary parts of a variable show its behaviour at the crest and the upwind slope of sinusoidal topography respectively.

Both the real and imaginary parts of the shear stress,  $\text{Re}(T)$  and  $\text{Im}(T)$ , and the perturbation velocity,  $\text{Re}(u)$  and  $\text{Im}(u)$ , coincide with their numerical predictions fairly well up to a height where  $\hat{\eta} = O(10)$ . In contrast, BNH's analytical results showed a poor prediction of the imaginary part of the complex amplitude of the shear stress  $\text{Im}(T)$ , and they suggested that the mixing-length model is less accurate at the upwind slope because turbulent advection is strong enough to influence the Reynolds stresses. Accordingly, we attribute the improvement of our prediction to the incorporation of eddy advection by using the viscoelastic model. Furthermore, our model reduces the dip at the top of the inner layer ( $\hat{\eta} = O(1)$ ) where the perturbation velocity  $u$  reaches its maximum value. We therefore conjecture that this dip in Reynolds stress is mainly an effect of turbulent advection.

From figure 12, which shows  $\text{Re}(T)$  and  $\text{Im}(T)$  on a linear vertical scale, we note the similarity to the well-known solution for a laminar oscillatory boundary layer (cf.

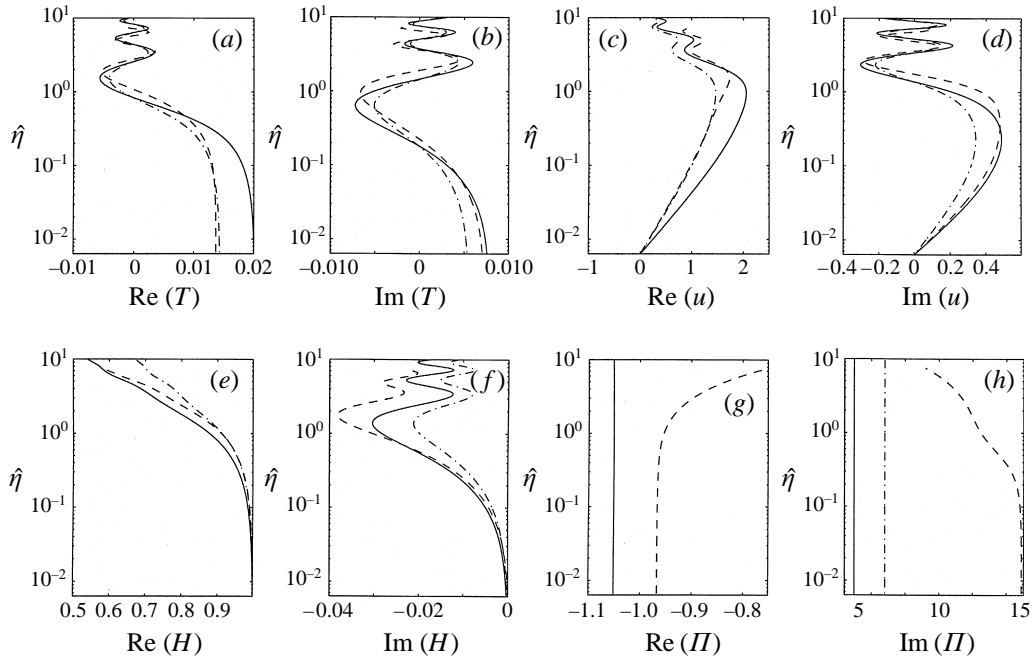


FIGURE 6. Comparisons of analytical and numerical results for a roughness length  $\eta_0 = 2 \times 10^{-4}$  and  $n = 0$  ( $l \approx 0.03$ ,  $\delta \approx 0.20$ ,  $\varepsilon \approx 0.12$ ): —, analytical solutions with matching coefficient (3.35a); ---, analytical solutions with matching coefficient (3.35b); -·-, numerical calculation. (a)  $\text{Re}(T)$ , (b)  $\text{Im}(T)$ , (c)  $\text{Re}(u)$ , (d)  $\text{Im}(u)$ , (e)  $\text{Re}(H)$ , (f)  $\text{Im}(H)$ , (g)  $\text{Re}(II)$ , (h)  $\text{Im}(II)$ .

Lamb 1945, p. 620). The oscillations decay with distance from the no-slip boundary. This oscillation is absent for isolated topography (see figure 8). Thus we propose that the oscillatory behaviour reflects the horizontal spatial modulation of turbulent flow by the sinusoidal topography.

The real parts of analytical solutions  $\text{Re}(H)$  and  $\text{Re}(II)$  agree well with their numerical calculations, whereas the imaginary parts  $\text{Im}(H)$  and  $\text{Im}(II)$  give satisfactory predictions only in the lower and upper part of the inner layer respectively. As also shown in figure 5, the analysis underestimates the numerical value of  $\text{Im}(II)$  by a factor 2 at the surface. According to their analytical solutions (3.13) and (3.35) and numerical results in figure 5(f, h),  $\text{Im}(H)$  and  $\text{Im}(II)$  are  $O(\delta^2)$ , and their analytical solutions are approximations with an error factor  $1 + O(\delta)$ . Figure 5(g) confirms that taking  $\text{Re}(II)$  as a constant is a good approximation, whereas figure 5(h) shows that  $\text{Im}(II)$  increases by a factor 2 from the top to the bottom of inner layer. Our drag force formula, based on the assumption of constant pressure in the inner layer, therefore underestimate the drag force by a factor 2. This may have caused theoretical predictions of drag force and wave growth rate to be smaller than observation results.

To study how the comparisons change with the small parameters  $\varepsilon$  and  $\delta$ , we follow the same procedure for the roughness length  $\eta_0 = 2 \times 10^{-4}$  and  $n = 0$  ( $l \approx 0.03$ ,  $\delta \approx 0.20$ ,  $\varepsilon \approx 0.12$ ), and the results are illustrated in figure 6. It is evident that nothing fundamental changes except that the analytical and numerical curves do not overlap each other as well as in figure 5. We find that this deficit is enlarged dramatically when  $\eta_0 \rightarrow 2 \times 10^{-2}$  ( $\delta \rightarrow 0.6$ ,  $\varepsilon \rightarrow 0.50$ ), which suggests that the prediction could be improved by including higher-order terms of  $O(\varepsilon^2, \mu^2)$  in the asymptotic analysis. Nevertheless, these figures strongly suggest that our analysis provides a good approximation for

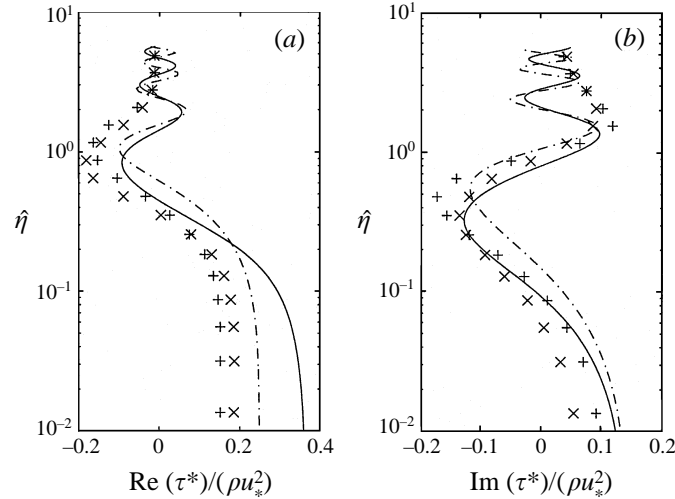


FIGURE 7. Comparisons of perturbation shear stress profiles at (a) the crest and (b) the upwind slope of a sinusoidal topography ( $k = \frac{1}{2}\pi$ ,  $\mu = 0.04$ ,  $\eta_0 = 4 \times 10^{-4}$ ): —, the present analytical solutions ( $n = 0$ ) with matching coefficient (3.35a); --, the present numerical computations;  $\times$ , +, BNH's numerical predictions using a second-order closure model.

relatively large  $\varepsilon$  and  $\delta$ , and certainly over the ranges in which we are interested (typical values of  $\varepsilon$  are 0.03–0.07 in the atmospheric boundary layer).

Figures 7(a) and 7(b) show a comparison of shear stress at the crest and the upwind slope of sinusoidal topography ( $k = \frac{1}{2}\pi$ ,  $\mu = 0.04$ ,  $\eta_0 = 4 \times 10^{-4}$ ), calculated by the present analytical and numerical modelling and BNH's numerical computations using a second-order closure model. Considering  $\delta \approx 0.25$  here, our analytical and numerical calculations both predict the shear stress fairly well. We note that at the crest, the analytical solution gives a surface shear stress that is about twice that of BNH's numerical modelling; at the upper wind slope, it provides a good approximation.

In figure 8, we demonstrate how well the present model predicts the shear stress at the top of a hill. The comparison is made between the present analytical and numerical studies, BNH's second-order closure model and the observational results at Askevein (Zeman & Jensen 1987), Nyland hill (Mason 1986) and Blashval (Mason & King 1985) (BNH, figure 8). We apply our analysis to Askevein with a shape defined by  $h_B(\xi) = \exp(-\xi^2 \log 2)$ , a roughness length  $\eta_0 = 4 \times 10^{-5}$ , but with a different slope  $\mu = 0.1$ .

Both analytical and numerical computations predict a small perturbation of shear stress in the outer region  $\eta = O(1)$  and a dip at the top of the inner layer  $\eta = O(l)$ , which agrees well with BNH's second-order closure model and field measurements. On the other hand, they give a prediction that is about three times those of observations near the surface. This disagreement may be caused by applying our linear analysis to steep hills ( $\mu = 0.4$ –0.5) and using a constant roughness length. The measurements near the surface are not as reliable either. It is worth remarking that the previously observed oscillation of shear stress is absent in this case.

Figure 9 shows the comparison of shear stress profiles at the crest and the upwind slope of a propagating water wave, using the present model and Hsu, Hsu & Street's (1981) measurements (their figure 5). Hsu *et al.* studied a travelling wave with wavenumber, amplitude and phase speed of  $k = 0.04 \text{ cm}^{-1}$ ,  $a = 2.67 \text{ cm}$ , and  $c = 156 \text{ cm s}^{-1}$  blown by wind with a friction velocity  $u_* = 8.5 \text{ cm s}^{-1}$  and a roughness



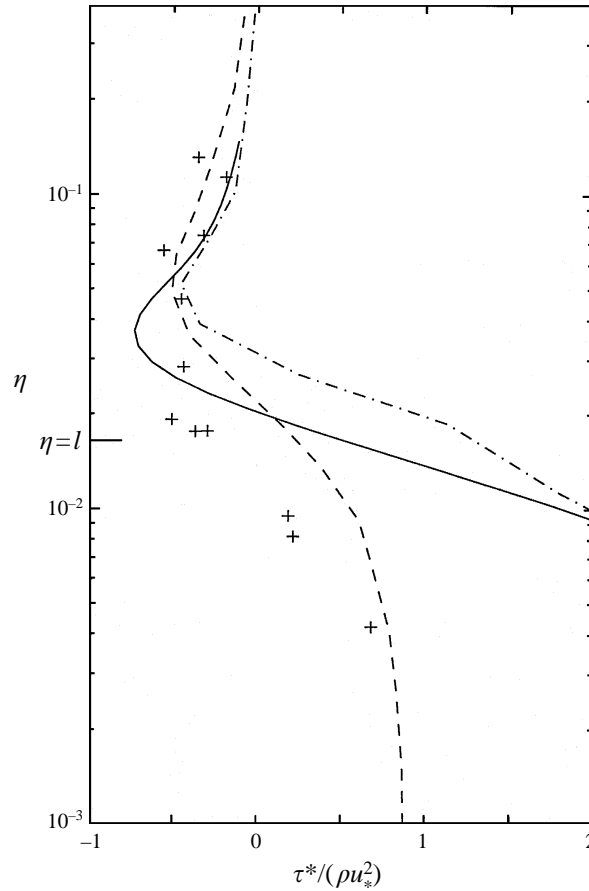


FIGURE 8. Comparisons of perturbation shear stress profiles at the summit of an isolated hill: —, analytical solutions ( $n = 0$ ,  $\eta_0 = 4 \times 10^{-5}$ ,  $\mu = 0.1$ ) with matching coefficient (3.35a); -·-, present numerical computation; ---, BNH's numerical predictions using a second-order closure model; +, field data collected at Askevein (Zeman & Janssen 1987), Nyland hill (Mason 1986) and Blashval (Mason & King 1985) (cf. BNH's figure 8).

length  $z_0 = 0.02$  cm; we then derived a matched height  $z_m = 0.08$  cm and its non-dimensional value  $\eta_m = 0.02$  with respect to a quarter of the wavelength. Despite the disagreement in magnitude between theory and experiment, the present model is able to capture the trend of Hsu *et al.*'s observations. Taking into account that  $\delta \approx 0.6$  here, this is a good comparison. In addition, we extend our theory of sinusoidal topography directly to a travelling wave with a roughness length  $\eta_0 = \eta_m$ .

To study how the value of  $\alpha$ , the weight parameter of eddy advection, affects the results, in figure 10 we plot the numerical computations for the roughness length  $\eta_0 = 2 \times 10^{-4}$  and  $n = 0$  ( $l \approx 0.03$ ,  $\delta \approx 0.20$ ,  $\varepsilon \approx 0.12$ ) at  $\alpha = 1/0.15$ ,  $\alpha = 1/0.3$  and  $\alpha = 0$ . It is worth mentioning that  $\alpha = 0$  curves correspond to omitting eddy advection entirely and using an eddy-viscosity model through the whole domain. Figure 12 shows that as  $\alpha = 1/0.15 \rightarrow 1/0.3$ , the magnitude changes; whereas as  $\alpha = 1/0.15 \rightarrow 0$ , both the magnitude and characteristics change dramatically. Hence, this plot gives strong evidence that eddy advection should be included in the modelling of this problem.

Finally, a comparison of numerical computations using the present viscoelastic

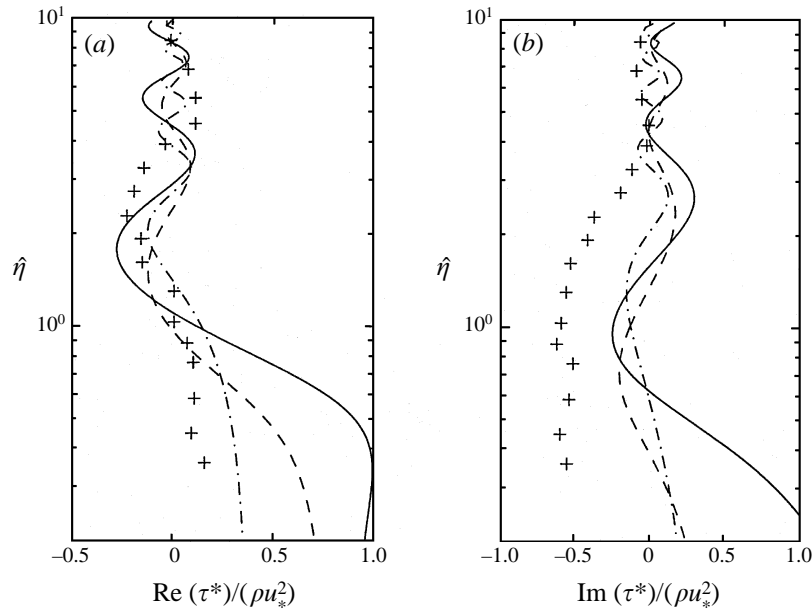


FIGURE 9. Comparisons of perturbation shear stress profiles (a) at the crest and (b) at the upwind slope of a sinusoidal water wave (cf. Belcher & Hunt's figure 10): —, the present analytical solutions ( $n = 0$ ,  $\eta_0 = 2 \times 10^{-2}$ ,  $\delta \approx 0.6$ ) with matching coefficient (3.35 a); ---, the present numerical computations; +, Hsu *et al.*'s (1981) experimental observations.

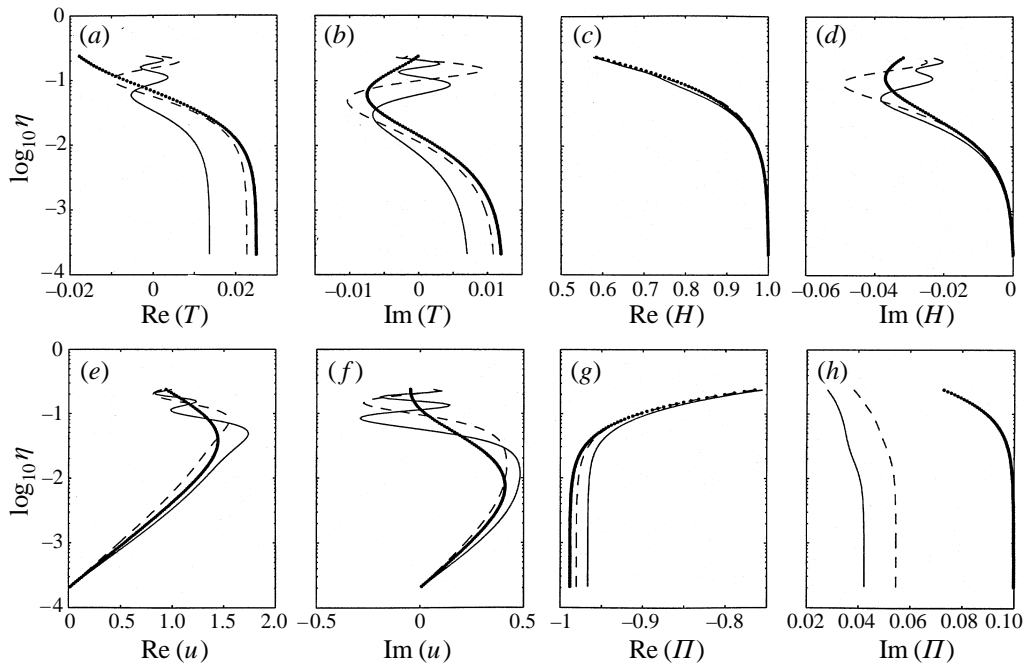


FIGURE 10. Comparisons of numerical results for a roughness length  $\eta_0 = 2 \times 10^{-4}$  and  $n = 0$  ( $l \approx 0.03$ ,  $\delta \approx 0.20$ ,  $\varepsilon \approx 0.12$ ): present model with —,  $\alpha = 1/0.15$ ; ---,  $\alpha = 1/0.3$ ;  $\cdots$ ,  $\alpha = 0$  (omitting eddy advection totally and using eddy-viscosity models in both outer and inner layers). (a)  $\text{Re}(T)$ , (b)  $\text{Im}(T)$ , (c)  $\text{Re}(H)$ , (d)  $\text{Im}(H)$ , (e)  $\text{Re}(u)$ , (f)  $\text{Im}(u)$ , (g)  $\text{Re}(II)$ , (h)  $\text{Im}(II)$ .

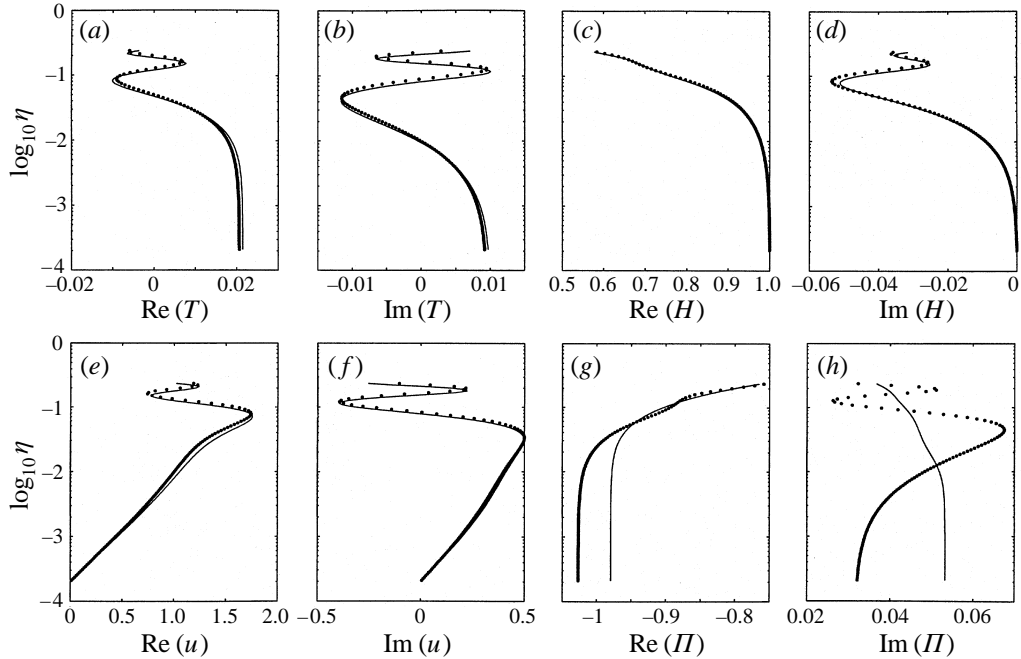


FIGURE 11. Comparisons of numerical results for a roughness length  $\eta_0 = 2 \times 10^{-4}$  and  $n = 1$ : —, present model (2.12a, b);  $\cdots$ , model (A 5a) and (A 6a, b) derived from Townsend's (1972) turbulent energy equation. (a)  $\text{Re}(T)$ , (b)  $\text{Im}(T)$ , (c)  $\text{Re}(H)$ , (d)  $\text{Im}(H)$ , (e)  $\text{Re}(u)$ , (f)  $\text{Im}(u)$ , (g)  $\text{Re}(II)$ , (h)  $\text{Im}(II)$ .

model (2.12a, b) and the modified Townsend turbulent model (A 5a) and (A 6a, b) is displayed in figure 11. The two sets of curves overlap well except for the pressure profiles. This difference reflects the fact that the two models define normal stresses differently (cf. (2.12b) and (A 6a, b)). We recall that normal Reynolds stresses are ignored in our analytical analysis, so that (A 5a) and (A 6a, b) give the same analytical solutions. Furthermore, our analysis predicts a surface asymmetric pressure about half that of the present numerical model (see figure 5h and figure 6h), as do the numerical results of (A 5a) and (A 6a, b) (figure 11h). We therefore conjecture that these two compare better with each other and that the normal stress formula (A 6a, b) represent the pressure and normal stresses near the surface better than (2.12b).

## 8. Discussion and conclusions

We have constructed a viscoelastic model that allows us to calculate the effect of eddy advection both analytically and numerically. Our analyses are carried out through matched asymptotic expansions, and our numerical computations through a shooting method. From both analyses and numerical computations, we predict a dip in shear stress near the interface between the inner and outer layers (see figure 5a, b and figure 6a, b). This feature has been noted in numerical models and verified by field observations but not in analytical models, and it has dynamical significance for this problem (see Zeman & Jensen 1987). The present model provides quantitative evidence that this feature is related to eddy convection which most previous authors neglect (see BNH).

The present model also reveals that the Reynolds shear stress oscillates in that region

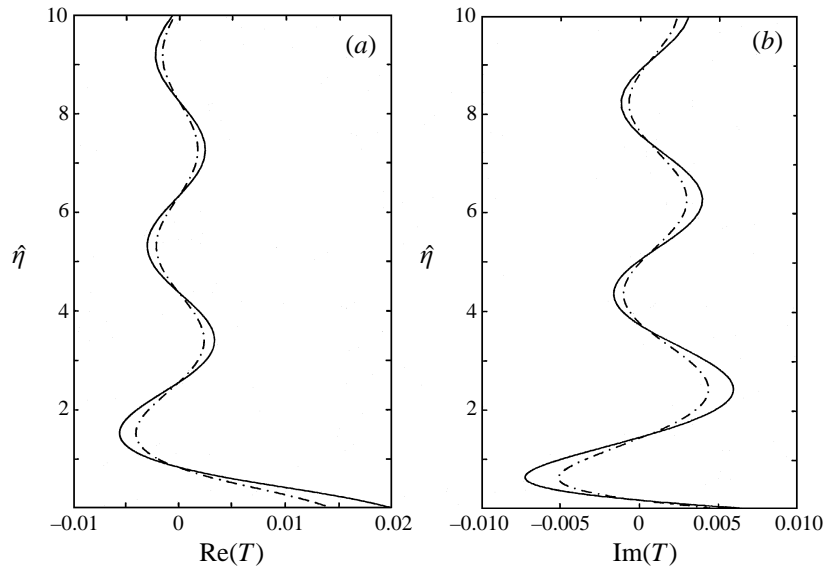


FIGURE 12. (a) Same as figure 6(a) except for the linear vertical coordinate. (b) Same as figure 6(b) except for the linear vertical coordinate.

and dies away far from the surface. This oscillatory behaviour reflects the horizontal spatial modulation of turbulent flow by the sinusoidal topography. As illustrated in figure 12, it seems analogous to the oscillation in viscous stress with height above an oscillating plate. This feature, however, has not been detected by any previous models or observation and warrants further investigation.

In §5, we calculated the leading-order drag force contributed by the Reynolds stresses and found it vanishes if  $n = 0$  (eddy-viscosity models); otherwise, it has the same magnitude as that contributed by asymmetric pressure (e.g. mixing-length models). This result suggests caution in accepting drag-force formulas that only include the effect of asymmetric pressure.

The present analysis using the matched asymptotic method gives a good approximation of the vertical structure of turbulent flow in this problem (see figure 5); however, similar to previous eddy-viscosity models, it underestimates the asymmetric pressure,  $\text{Im}(II)$ , at the surface. Although neglecting the vertical pressure gradient is a conventional practice in the analysis of this problem, it could cause considerable underestimation of the asymmetric pressure (see figures 5*h* and 6*h*). As discussed in §7, a higher-order analysis of  $O(\varepsilon^2, \mu^2)$  including vertical pressure gradient and nonlinearity is expected to give a better prediction of this problem.

In their recent paper, Belcher & Hunt (1993) extended BNH's and HLR's analysis to turbulent flow over slowly travelling waves. We have extended our theory of turbulent flow over a hill to turbulent flow over progressive water waves (cf. Zou 1995, Chap. 1, §8) and found a fair agreement between wave growth rate predicted by the present theory and Plant's (1982) compilation of observation data. In contrast to Belcher & Hunt, we use a roughness length depending on wave age and take the critical layer into account. Further research on this topic should be carried out.

This work was done as part of my PhD thesis while at Scripps Institution of Oceanography. Above of all, I wish to thank my thesis advisor John Miles for drawing my attention to this problem, and for his help with its presentation. I also want to

thank Steve Belcher for providing BNH's numerical results and his valuable comments on this manuscript, Owen M. Phillips for helpful suggestions, and Alan Brandt, Haydee Salmun for encouraging me to submit this paper. I am grateful to the anonymous reviewers and editor for their criticisms that helped to improve the original manuscript. This work was supported in part by the Division of Ocean Sciences of the National Science Foundation, NSF Grant OCE95-01508 and by the Office of Naval Research Grant N00014-92-J-1171.

### Appendix A. A viscoelastic model

We consider Townsend's turbulent energy equation (Townsend 1976, §7.13)

$$\frac{u}{2a_1} \left( \frac{\partial \tau}{\partial z} \right)_\phi = -\frac{\partial}{\partial z} (\langle p'w' \rangle + \frac{1}{2} \langle q^2 w' \rangle) + \tau \frac{\partial u}{\partial z} - a_1^{-3/2} \tau^{3/2} L_e^{-1}, \quad (\text{A } 1)$$

where  $z$  is the transverse coordinate,  $\phi$  is the stream function,  $L_e$  is the dissipation length scale,  $\langle \rangle$  implies averaging, a prime signifies fluctuating variables,

$$a_1 = -\frac{\langle u'w' \rangle}{q^2} = 0.15, \quad (\text{A } 2)$$

and  $q^2$  is the turbulent kinetic energy. The left-hand-side term of (A 1) stands for the advected turbulent energy along a streamline of the stream function, and the right-hand-side terms represent diffusion, production and dissipation of turbulent energy respectively.

Neglecting diffusion (see Bradshaw *et al.* 1967), decomposing the other two right-hand-side terms into the zeroth-order and perturbation components, i.e.

$$\tau \frac{\partial u}{\partial z} = \tau_0 U_z + \tau_0 \left( \frac{\partial u}{\partial z} - U_z \right) + (\tau - \tau_0) U_z + O(\delta\tau \delta u_z), \quad (\text{A } 3a)$$

$$\tau^{3/2} = \tau_0^{3/2} + \frac{3}{2} \tau_0^{1/2} (\tau - \tau_0) + O((\delta\tau)^2), \quad (\text{A } 3b)$$

substituting (A 3a) and (A 3b) into (A 1), at the zeroth-order we have

$$\tau_0^{1/2} \frac{\partial U}{\partial z} = \frac{a_1^{3/2} \tau_0^{3/2}}{L_e}, \quad (\text{A } 4a)$$

which reduces to

$$L_e = \frac{a_1^{-3/2} \tau_0}{\partial U / \partial z}, \quad (\text{A } 4b)$$

and at the first-order we have

$$\frac{1}{a_1} \frac{D\tau}{Dt} + U_z (\tau - \tau_0) = 2\tau_0 \left( \frac{\partial u}{\partial z} - U_z \right), \quad (\text{A } 5a)$$

where  $\tau_0 = \nu_0 U_z$  is the zeroth-order shear stress. We assume a steady flow and invoke  $D/Dt = u \partial / \partial \xi|_\phi$ . Introducing a relaxation time  $T_e = 1/(a_1 U_z)$  and an effective eddy viscosity  $\nu = 2\nu_0$ , we further transform (A 5a) into

$$T_e = \frac{D\tau}{Dt} + (\tau - \tau_0) = \nu \left( \frac{\partial u}{\partial z} - U_z \right) \quad (\text{A } 5b)$$

which is identified as a viscoelastic model with  $n = 1$  (see (2.12a)). According to Townsend (1976), near the surface, the ratios between Reynolds stresses are constants with approximate values

$$\alpha_1 = \frac{-\langle u'^2 \rangle}{\langle u'w' \rangle} = 6.3 \quad \text{and} \quad \alpha_2 = \frac{-\langle w'^2 \rangle}{\langle u'w' \rangle} = 1.7. \quad (\text{A } 6a, b)$$

This modelling is verified by both field data and numerical computations (Bradshaw *et al.* 1967; Zeman & Jensen 1987). We assume that relationships (A 6a, b) are valid throughout the inner domain.

### Appendix B. The first-order equations

The first-order equations are

$$\frac{d \operatorname{Re}(H)}{d\eta} = \operatorname{Re}(H_\eta), \quad \frac{d \operatorname{Im}(H)}{d\eta} = \operatorname{Im}(H_\eta), \quad (\text{B } 1 a, b)$$

$$\frac{d \operatorname{Re}(H_\eta)}{d\eta} = -\frac{1}{U} \left[ \operatorname{Re}(T) \operatorname{Re}\left(\frac{1}{\nu}\right) - \operatorname{Im}(T) \operatorname{Im}\left(\frac{1}{\nu}\right) \right] - \frac{2U_\eta}{U} \operatorname{Re}(H_\eta) - \frac{k^2}{n+1} \operatorname{Re}(H), \quad (\text{B } 1 c)$$

$$\frac{d \operatorname{Im}(H_\eta)}{d\eta} = -\frac{1}{U} \left[ \operatorname{Im}(T) \operatorname{Re}\left(\frac{1}{\nu}\right) + \operatorname{Re}(T) \operatorname{Im}\left(\frac{1}{\nu}\right) \right] - \frac{2U_\eta}{U} \operatorname{Im}(H_\eta) - \frac{k^2}{n+1} \operatorname{Im}(H), \quad (\text{B } 1 d)$$

$$\frac{d \operatorname{Re}(T)}{d\eta} = kU^2 \operatorname{Im}(H_\eta) - k \operatorname{Im}(II) + k \operatorname{Im}(\Sigma), \quad (\text{B } 1 e)$$

$$\frac{d \operatorname{Im}(T)}{d\eta} = -kU^2 \operatorname{Re}(H_\eta) + k \operatorname{Re}(II) - k \operatorname{Re}(\Sigma), \quad (\text{B } 1 f)$$

$$\frac{d \operatorname{Re}(II)}{d\eta} = k^2 U^2 \operatorname{Re}(H) - \operatorname{Re}(\Sigma_\eta) - k \operatorname{Im}(T), \quad (\text{B } 1 g)$$

$$\frac{d \operatorname{Im}(II)}{d\eta} = k^2 U^2 \operatorname{Im}(H) - \operatorname{Im}(\Sigma_\eta) + k \operatorname{Re}(T), \quad (\text{B } 1 h)$$

where

$$\operatorname{Re}(\Sigma) = \frac{2k}{n+1} [\operatorname{Im}(\nu) (U_\eta \operatorname{Re}(H) + U \operatorname{Re}(H_\eta)) + \operatorname{Re}(\nu) (U_\eta \operatorname{Im}(H) + U \operatorname{Im}(H_\eta))], \quad (\text{B } 2 a)$$

$$\operatorname{Im}(\Sigma) = -\frac{2k}{n+1} [\operatorname{Re}(\nu) (U_\eta \operatorname{Re}(H) + U \operatorname{Re}(H_\eta)) - \operatorname{Im}(\nu) (U_\eta \operatorname{Im}(H) + U \operatorname{Im}(H_\eta))], \quad (\text{B } 2 b)$$

$$\operatorname{Re}(\Sigma_\eta) = \frac{2k}{(n+1)} [\operatorname{Im}(\nu_\eta) (U_\eta \operatorname{Re}(H) + U \operatorname{Re}(H_\eta)) + \operatorname{Re}(\nu_\eta) (U_\eta \operatorname{Im}(H) + U \operatorname{Im}(H_\eta)) \\ + U_{\eta\eta} (\operatorname{Im}(\nu) \operatorname{Re}(H) + \operatorname{Re}(\nu) \operatorname{Im}(H)) - \operatorname{Im}(T)], \quad (\text{B } 2 c)$$

$$\operatorname{Im}(\Sigma_\eta) = -\frac{2k}{n+1} [\operatorname{Re}(\nu_\eta) (U_\eta \operatorname{Re}(H) + U \operatorname{Re}(H_\eta)) - \operatorname{Im}(\nu_\eta) (U_\eta \operatorname{Im}(H) + U \operatorname{Im}(H_\eta)) \\ + U_{\eta\eta} (\operatorname{Re}(\nu) \operatorname{Re}(H) - \operatorname{Im}(\nu) \operatorname{Im}(H)) - \operatorname{Re}(T)], \quad (\text{B } 2 d)$$

$$\operatorname{Re}(\nu) = \frac{(n+1)(\varepsilon\kappa)^2 U_\eta}{U_\eta^2 + (k\alpha U)^2}, \quad \operatorname{Im}(\nu) = \frac{-(n+1)(\varepsilon\kappa)^2 k\alpha U}{U_\eta^2 + (k\alpha U)^2}, \quad (\text{B } 3 a, b)$$

$$\operatorname{Re}(\nu_\eta) = \frac{-(n+1)(\varepsilon\kappa)^2 U_\eta}{[U_\eta^2 + (k\alpha U)^2]^2} \{ U_{\eta\eta} [U_\eta^2 - (k\alpha U)^2] + 2(k\alpha U_\eta)^2 U \} \quad (\text{B } 3 c)$$

and

$$\text{Im}(\nu_\eta) = \frac{-(n+1)(\epsilon\kappa)^2 k\alpha U_\eta}{[U_\eta^2 + (k\alpha U)^2]} [U_\eta^2 - (k\alpha U)^2 - 2UU_\eta]. \quad (\text{B } 3d)$$

#### REFERENCES

- ABRAMOWITZ, M. & STEGUN, I. A. 1970 *Handbook of Mathematical Functions*. US National Bureau of Standards.
- BELCHER, S. E. & HUNT, J. C. R. 1993 Turbulent shear flow over slowly moving waves. *J. Fluid Mech.* **251**, 109–148.
- BELCHER, S. E., NEWLEY, T. M. J. & HUNT, J. C. R. 1993 The drag on an undulating surface induced by the flow of a turbulent boundary layer. *J. Fluid Mech.* **249**, 557–596 (referred to herein as BNH).
- BRADSHAW, P., FERRIS, D. H. & ATWELL, N. P. 1967 Calculation of boundary layer development using the turbulent kinetic energy equation. *J. Fluid Mech.* **30**, 241–258.
- BRITTER, R. E., HUNT, J. C. R. & RICHARDS, K. J. 1981 Air flow over a 2-d hill: studies of velocity speed-up roughness effects and turbulence. *Q. J. R. Met. Soc.* **107**, 91–110.
- DAVIS, R. E. 1972 On prediction of the turbulent flow over a wavy boundary. *J. Fluid Mech.* **52**, 287–306.
- DRAZIN, P. G. & REID, W. H. 1981 *Hydrodynamic Stability*. Cambridge University Press.
- DUIN, C. A. VAN & JANSSEN, P. A. E. M. 1992 An analytical model of the generation of surface gravity waves by turbulent air flow. *J. Fluid Mech.* **236**, 197–215.
- HUNT, J. C. R., LEIBOVICH, S. & RICHARDS, K. J. 1988 Turbulent shear flow over hill. *Q. J. R. Met. Soc.* **114**, 1435–1470 (referred to herein as HLR).
- HSU, C. T., HSU, E. Y. & STREET, R. L. 1981 On the structure of turbulent flow over a progressive water wave: theory and experiment in a transformed wave, following coordinate system. *J. Fluid Mech.* **105**, 87–118.
- JACKSON, P. S. & HUNT, J. C. R. 1975 Turbulent wind flow over a low hill. *Q. J. R. Met. Soc.* **101**, 929–955.
- JACOBS, S. J. 1987 An asymptotic theory for the turbulent flow over a progressive water wave. *J. Fluid Mech.* **174**, 69–80.
- JACOBS, S. J. 1989 Effective roughness length for turbulent flow over a wavy surface. *J. Phys. Oceanogr.* **19**, 998–1010.
- JENKINS, A. D. 1992 A quasi-linear eddy-viscosity model for the flux of energy and momentum to wind waves using conservation-law equations in a curvilinear coordinate system. *J. Phys. Oceanogr.* **22**, 843–858.
- KAIMAL, J. C. & FINNIGAN, J. J. 1994 *Atmospheric Boundary Layer Flows – Their Structure and Measurement*. Oxford University Press.
- KNIGHT, D. 1977 Turbulent flow over a wavy boundary. *Boundary-Layer Met.* **11**, 209–222.
- LAMB, H. 1945 *Hydrodynamics*. Dover.
- MASON, P. J. & KING, J. C. 1985 Measurements and prediction of flow and turbulence over an isolated hill of small slope. *Q. J. R. Met. Soc.* **111**, 617–640.
- MILES, J. W. 1993 Surface-wave generation revisited. *J. Fluid Mech.* **256**, 427–441.
- OLVER, F. W. J. 1974 *Asymptotics and Special Function*. Academic.
- PHILLIPS, O. M. 1977 *The Dynamics of the Upper Ocean*, 2nd edn. Cambridge University Press.
- PLANT, W. J. 1982 A relationship between wind stress and wave slope. *J. Geophys. Res.* **87**, 1961–1967.
- RIVLIN, R. S. 1957 The relation between the flow of non-Newtonian fluids and turbulent Newtonian fluids. *Q. Appl. Maths* **15**, 212–215.
- SAFFMAN, P. G. 1977 Results of a two-equation model for turbulent flows and development of a relaxation stress model for application to straining and rotating flows. *Proc. Project SQUID Workshop Turbulence in Internal Flows* (ed. S. Murphy), pp. 191–231. Hemisphere.
- SANFORD, M. R. & SHIPMAN, J. S. 1972 *Two-Point Boundary Value Problems: Shooting Method*. Elsevier.

- SPEZIALE, C. G. 1987 On nonlinear  $K-l$  and  $K-\varepsilon$  models of turbulence. *J. Fluid Mech.* **178**, 459–475.
- SPEZIALE, C. G. 1991 Analytical methods for the development of Reynolds-stress closures in turbulence. *Ann. Rev. Fluid Mech.* **23**, 107–157.
- SYKES, R. I. 1980 An asymptotic theory of incompressible turbulent flow over a small hump. *J. Fluid Mech.* **101**, 647–670.
- TENNEKES, H. & LUMLEY, J. L. 1992 *A First Course in Turbulence*. The MIT Press.
- TOWNSEND, A. A. 1972 Flow in a deep turbulent boundary layer over a surface distorted by water waves. *J. Fluid Mech.* **55**, 719–735.
- TOWNSEND, A. A. 1976 *The Structure of Turbulent Shear Flow*. Cambridge University Press.
- ZEMAN, O. & JENSEN, N. O. 1987 Modification to turbulence characteristics in flow over hills. *Q. J. R. Met. Soc.* **113**, 55–80.
- ZILKER, D. P. & HANRATTY, T. J. 1979 Influence of the amplitude of a solid wavy boundary on a turbulent flow. Part 2. Separated flows. *J. Fluid Mech.* **90**, 257–271.
- ZOU, Q.-P. 1995 A viscoelastic model for turbulent flow over undulating topography and progressive waves, PhD thesis, Scripps Institution of Oceanography, University of California at San Diego.